Politecnico di Torino

Master's Degree in Electronic Engineering

Master's Degree Thesis

Laser Annealing On Wafer

Supervisors

Prof. Luciano Scaltrito

Prof. Sergio Ferrero

Candidate

Jiajun Qiao

October 2021

Abstract

The integrated circuit (IC) was little known before the 1960s. However, today in 2021, it is said that the integrated circuit is the product of civilisation with the fastest progress in human science and technology in this century. Before the invention of the integrated circuit, human beings lived in an era of information scarcity. After the invention of the integrated circuit, people lived in an age of information explosion.

Moore's Law[1]points out that the line width of the circuit within the IC is rapidly narrowing, and the difference in thickness is only 1/10 of the line width. This design specification makes the line width of the IC circuit smaller, and it is difficult to distinguish between the current signal and the current noise accurately. As there are more and more transistors and the size is getting smaller, the difficulty of the manufacturing process of the transistors is significantly increased. With the continuous reduction of the feature size of integrated circuits and the constant increase of the number of transistors, large-size wafers have put forward further requirements for annealing methods.

The energy-saving is leading new design paradigms and processing steps to the fabrication of discrete power devices. Main activities minimise the bulk material where most of the energy is dissipated during switching time. The thesis will focus on studying a post-implantation process; in particular, a particular laser source will be designed, and a scanner system will be implemented to exploit the laser annealing process in two different wavelengths.

Contents

List of Figures

List of Tables

Chapter 1 Introduction

The first chapter aims to introduce the annealing history and methods briefly.

1.1 Annealing

According to the type of doped atoms, two types of wafers can be obtained: n-type or p-type. High-energy incident ions collide with atoms on the semiconductor lattice when impurity ions are implanted into a semiconductor. This will cause displacement of atoms and create a large number of vacancies, which will lead to the disordered arrangement of atoms in the implanted area or become amorphous. Then cause low activation efficiency of impurities and a decrease in electron mobility. Therefore, the semiconductor after ion implantation must be annealed at a specific temperature to restore the crystal structure and eliminate defects. At the same time, annealing also activates donor and acceptor impurities [2]. That is, annealing makes some impurity atoms in interstitial positions to allow them to enter replacement positions.

With the development of integrated circuits, the requirements for the damaged area, the recovery of electrical parameters, and the electrical activation rate of implanted ions are getting stricter. The conventional thermal annealing methods can no longer meet the requirements. Because it cannot eliminate defects, the electrical activation rate for high-dose implanted wafers is not high enough, producing secondary defects [3]. At the same time, during the thermal annealing process, the entire wafer (including the implanted layer and the substrate) has to undergo a high-temperature treatment, which increases surface contamination. In particular, high temperature and long-term thermal annealing will cause the significant redistribution of impurities [4] and destroy ion implantation. The shortcomings of thermal annealing technology limit its application in VLSI. The annealing method has been extensively studied for many years to solve the above problems, leading to the emergence of rapid annealing technologies such as laser annealing.

Rapid thermal annealing (RTA) uses various heat radiation sources to irradiate the sample's surface directly and quickly heat the sample to about 1400℃ in a few seconds to tens of seconds to complete the annealing. Compared with conventional thermal annealing, RTA has many advantages. Samples can be annealed at a higher temperature under protective conditions, which improves the activation rate and mobility of

implanted impurities. It is especially suitable for high-dose implantation samples because it is damaged severely and requires annealing at a higher temperature. Transient annealing can reduce the redistribution of implanted impurities and form a steep impurity distribution [5].

Rapid annealing technology currently includes pulsed lasers, pulsed electron beams, and ion beams, scanning electron beams, continuous-wave lasers, and broadband light sources (such as halogen lamps, arc lamps, graphite heaters). Their common feature is that a specific area of the wafer is heated to a very high temperature within an instant, then the annealing is completed in a short time.

1.2 Introduction to laser annealing

Laser annealing is currently the most widely used technology in the preparation of polysilicon materials. The method uses a high-power pulsed laser to act on amorphous silicon material. Then the surface of the amorphous silicon absorbs laser energy to raise the temperature to the phase transition temperature, cools and solidifies, and then converts it into polysilicon [6]. The laser light source has higher energy power, shorter wavelength, and shallow absorption depth in amorphous silicon materials. Therefore, this process has the characteristics of short annealing time and high crystallisation efficiency. In addition, the lower temperature at the substrate during the annealing process reduces the requirements on the substrate material, thereby reducing the manufacturing cost.

Generally speaking, energy density, pulse width, dwell time, and laser shape affects polysilicon crystal grains' crystallisation condition. The laser wavelength has a great relationship with the crystallisation effect [7].

Semiconductor silicon materials have become a hot spot in today's research due to lots of advantages. According to different crystal structures, silicon materials can be divided into amorphous silicon (a-Si), crystalline silicon (c-Si), and polycrystalline silicon (p-Si).

The carriers in crystalline silicon have high mobility, and the manufacturing cost of amorphous silicon is low. Polycrystalline silicon has the advantages of both crystalline silicon and amorphous silicon. [8].That is why polycrystalline are widely used in the field of optoelectronics. The difference between polycrystalline silicon and

monocrystalline silicon is mainly in physical properties. For example, in terms of mechanical and electrical properties, polycrystalline silicon is inferior to single crystal silicon. But in the semiconductor industry, monocrystalline silicon is often used

With the continuous development of the IC industry, the device's size continues to shrink, and the number of transistors integrated on the chip is increasing, which puts forward higher requirements for the annealing process. Compared with the traditional annealing process, laser annealing has many advantages. The spot size and spatial position of the laser light source are controllable. The sample can be locally annealed. The laser has a high energy density, which can significantly shorten the annealing time, and it can be lasered simultaneously. Compared with the traditional annealing method, the sample after laser annealing has larger grains and fewer defects, and the fabricated device has better electrical properties.

Chapter 2 Laser system

In this chapter, the development history and basic theory of lasers are introduced. Meanwhile, two types of lasers used in experiments are introduced.

2.1 Introduction to laser

2.1.1 The critical history of laser

The word 'LASER' comes from the Light Amplification by Stimulated Emission of Radiation. Laser is another super invention of humankind since the 20th century. It is called "the fastest knife," "the most accurate ruler," and "the brightest light." [9] Its brightness is about 10 billion times that of sunlight.

The principle of the laser was discovered by the famous American physicist Einstein as early as 1917. However, it was not until 1960 that the laser was successfully manufactured for the first time.

In 1917 Albert Einstein pointed out the possibility of laser in his paper *Zur Undertheorize der Strahlung* (On the Quantum Theory of Radiation). After that, scientists made many efforts to study the laser.

In 1958, American scientists Schawlow and Townes discovered a phenomenon: when they put the light emitted by a neon bulb on a crystal, the molecules of the crystal will emit bright and intense light that always converges together. Based on this phenomenon, they proposed the "laser principle," that is, when a substance is excited by the energy of the same natural oscillation frequency as its molecule, it will produce this kind of non-divergent intense light—the laser. They published important papers for this and won the Nobel Prize in Physics in 1964.

In 1960, Theodore Maiman, a physicist from America, invented the first ruby laser with an operable wavelength of 0.6943 microns [10]. This laser was the first laser ever obtained in the world. For this reason, Maiman became the first scientist in the world to turn laser from theory to reality. At this time, it had been 43 years after Einstein proposed the laser theory. Furthermore, the New York Times first reported this news.

Few months after Theodore Maiman's ruby laser came out. Peter Sorokin and Mirek Stevenson, two engineers from the International Business Machines Corporation(IBM)

Watson Research Center, were greatly inspired by Maiman's ruby. According to the four-level laser system [11], the working medium doped with calcium fluoride is made into rectangular parallel tubes, and the surface is polished. The light goes back and forth in the solid block and finally exits from a cut corner. Since the refractive index of calcium fluoride (CaF_2) crystals doped with trivalent uranium ions(U^{3+}) and ions of divalent samarium (Sm^{2+}) is slightly greater than$\sqrt{2}$. So that the light can be reflected almost without loss after multiple round trips inside, both structures belong to a four-level laser. The system should work in a low-temperature state. Later, Peter Sorokin and Mirek Stevenson changed their crystals to cylindrical and plated with silver on the surface. In November 1960, they obtained the laser output of a CaF_2: U^{3+} four-level system, and in December, they ran a CaF_2: Sm^{2+} laser [12]. This laser was not visible light but infrared. Although the output power is smaller than ruby lasers, the graphics are clear and have good optical properties.

At the end of 1960, Javan, a thirty-four-year-old young Iranian engineer, finally obtained an infrared continuous laser oscillation with a wavelength of 1.15 microns through unremitting efforts. The result that Javan achieved means the beginning of Helium-neon (HeNe) gas lasers. Helium-neon gas laser is different from the pulse output of a solid-state laser. From this point of view, the helium-neon laser is a landmark in the laser's history. The output power is small but very stable, with good directivity and a small divergence angle.

On the one hand, it realises continuous oscillating output for the first time [13]. However, solid-state lasers are pulsed and not suitable for general use. Continuous laser beams broaden the application range of lasers. For this reason, helium-neon gas lasers have become the most widely used lasers in the past few decades. On the other hand, it is proved that the electric discharge method can generate the laser. As long as the appropriate energy level is selected in two different working media, it is possible to achieve light amplification, which shows the possibility of multiple realisation methods for manufacturing lasers.

In 1961, M.Clung and Hellwarth announced their successful use of Q-switching technology in lasers, which provided the possibility for high-energy and high-power lasers. In 1962, the idea of using semiconductors to generate laser light became a reality. The RDL laboratory of General Electric Company in the United States successfully

produced a diode laser. Then in October 1962, IBM engineer Nathan produced the first gallium arsenide (GaAs) semiconductor laser with a wavelength of about 8,400 angstroms. In the same year, Eckhard produced a Raman laser.

In 1964, Uitert, an engineer from Bell Laboratories, made a Neodymium-doped Yttrium Aluminum Garnet (Nd: YAG) laser. The gain of this kind of laser is huge, the threshold is low, and the thermal effect is small, so it has been widely used in scientific research and industrial applications. In the same year, Hargrove and his team Successfully developed a mode-locked laser. In July, Patel from Bell Laboratories successfully invented the world's first carbon dioxide gas molecular laser.

In 1970, Basov, a physicist in the former Soviet Union, made an excimer laser for the first time. His efforts are of great significance for subsequent research on vacuum ultraviolet lasers. In 1971, laser entered the world of art. The laser was used for stage light and shadow effects and laser holographic photography. Dennis Gabor, a Hungarian-British electrical engineer, and physicist won the Nobel Prize for his research on holographic photography.

Since then, many scientists have made outstanding contributions to the research and development of the laser field. By the end of the 1970s, breakthroughs had been made in laser characteristics. The lifetime of the laser has been dramatically extended, which could reach 50,000 to 100,000 hours. The continuous output power of carbon monoxide and carbon dioxide lasers can reach 100 watts to 250 kilowatts. Notably, a neodymium glass laser and a pulsed carbon dioxide laser have a power output of up to 100 million kilowatts (this number is much greater than the sum of the time of power stations worldwide).

In the last few years, the microelectronics manufacturing industry has been changed since lasers were introduced. In all aspects of electronic manufacturing, lasers can exhibit unique advantages. Figure 2.2.1 below shows some laser applications in the electronics industry.

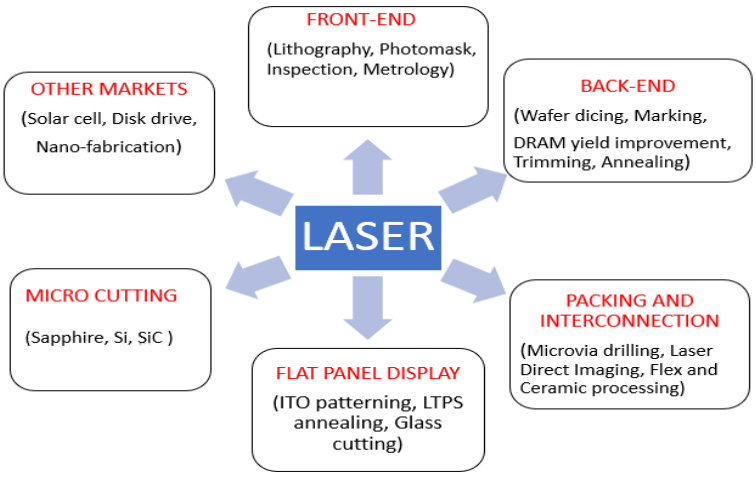

Figure 2.1.1 Laser applications in the electronics industry

2.1.2 The principle of laser

A laser is a device that uses the principle of stimulated emission to generate light and amplify light. The light emitted has excellent coherence, monochromaticity, directivity, and extremely high brightness, which is easy to control and use. The laser is a new type of light source produced based on human's long-term practice of improving the light source and continuous in-depth understanding of the nature of light. The emergence of lasers marks a leap in human understanding and utilisation of light.

The following section is excerpted from Principles of lasers [14].

The emission and absorption of light result from the action of the light with substances (atoms or molecules). The interaction of light with substances makes the atoms (or molecules in substances) jump from one energy level to another. It is accompanied by an increase or decrease of photons, which is the emission and absorption behaviour of individual atoms (or molecules) to light. This behaviour includes three basic processes: absorption of radiation, spontaneous emission, and stimulated emission.

These three interactions are briefly described below. Consider only the two energy levels E1 and E2 ($E_2 > E_1$) of the atoms.

- Radiation absorption

The electron in the ground state absorbs energy from the external photon. This energy causes the electron to jump from a low energy level(E_1) to a high energy level(E_2), called radiation absorption. The distance between the electrons and the nucleus causes an energy level difference between the electron energy levels. The electrons that are close to the nucleus are at a lower energy level. Conversely, electrons are further away from the nucleus when they are at higher energy levels. The stimulated absorption process only requires that the frequency of the external photon meets the formula (2.1.2), and there are no special requirements for its polarisation and direction. So, absorption of radiation is also called resonance absorption.

$$h\nu_{12} = E_2 - E_1 \tag{2.1.1}$$

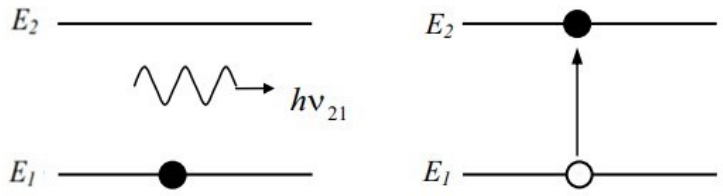

Figure 2.1.2 Absorption of radiation between two energy levels

- Spontaneous emission

It is defined as follows. The electrons in the high-energy level E_2, without external influence, spontaneously jump to the low-energy level E_1 and emits a photon with energy $h\nu_{21}$. This process is called spontaneous radiation. The energy of this photon is the energy difference between the two energy levels, and the process satisfies the formula (2.1.1). Generally, electrons at high energy levels (excited states) have very short lifetimes. It is uncontrollable when electrons jump to lower energy levels with emitting energy in the form of photons.

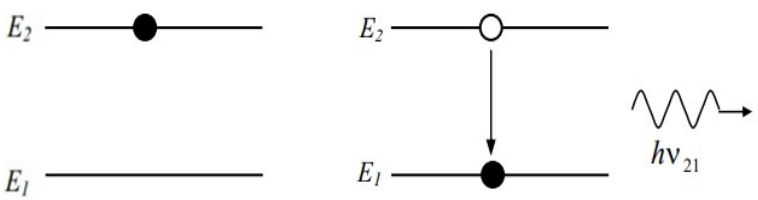

Figure 2.1.3 Spontaneous emission between two energy levels.

- Stimulated emission

Suppose an electron in energy level E_2 is subjected to an external light of frequency $h\nu_{21}$ ($h\nu_{21}$ satisfies equation (2.1.1). This electron may be excited by an external photon and drop from energy level E_2 to energy level E_1. At the same time, a photon of energy $h\nu_{21}$ is radiated.

Stimulated emission is very different from spontaneous emission. In spontaneous emission, electrons in an excited state will stay there until the end of their lifetime. After the electron's lifetime ends, the electron returns to the ground state by releasing energy in the form of light. In short, spontaneous emission is a spontaneous process.

Stimulated emission is the result of manual manipulation. In stimulated emission, electrons in an excited state do not need to wait for the end of their lifetime. The stimulated emission technology allows the electron to force the excited electron back to the ground state before the end of its life.

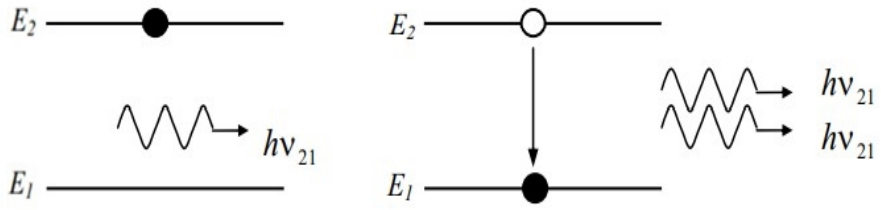

Figure 2.1.4 Stimulated emission between two energy levels.

It can be seen that in stimulated emission, two photons with the same energy (meaning the same frequency) and the same propagation direction are produced. One of them is the incident photon, and the other is the photon produced by excitation. The process of stimulated emission is much faster than the process of spontaneous emission.

2.1.3 The general structure of the laser

Lasers are classified into four types based on the type of laser medium used: solid-state laser, gas laser, liquid laser, and semiconductor laser. A laser device consists of three parts: laser medium, pump source, and optical resonator. The simplest solid-state laser diagram is as follows.

- Laser medium

To ensure stimulated emission becomes the primary process in the medium, the necessary condition is to cause the population inversion in the medium. Experiments have proved that various materials may generate laser light under certain external excitation conditions. These materials can be solids, gases, liquids, and semiconductors. Such materials that can generate laser light are called laser mediums. For example, the laser medium in the ruby laser is made of sapphire (Al_2O_3), which is doped with small amounts of chromium ions (Cr^{3+}). Choosing a suitable laser medium is the first prerequisite for manufacturing a laser. In order to select the suitable laser medium, the energy spectrum analysis of the material must be done. On this basis, the choice depends on different needs. Many other issues must be considered when chose a laser medium. The most important one is whether a material has suitable energy levels jump performance. That is, the population inversion can be achieved between two energy levels. The lifetime of the spontaneous emission of the upper energy level E_2 is generally required to be greater than the lifetime of the spontaneous emission of the lower energy level E_1.

In order to activate the laser medium, external excitation is required. The excitation methods include optical excitation, electrical excitation, and chemical excitation. Each kind of method requires an external excitation source, which is the pump source.

- Pump source

The pump source makes the particles in the ground state energy level in the medium continuously be promoted to the higher excited state energy level (this is called the pumping process), which causes the phenomenon of population inversion distribution in the medium. Of course, it should be pointed out that the population inversion distribution does not mean that all the higher energy levels have more particles than the lower energy levels. Generally, the population inversion distribution only occurs between a certain (or some) higher energy level(s) and a certain (or some) lower energy level(s).

The choice of pump source depends on the characteristics of the laser medium. Therefore, different materials often require different pump sources. For example, for solid-state lasers, pulsed xenon lamps or iodine tungsten lamps are generally used. While for gas lasers, electrical excitation methods are used to excite the laser medium

through discharge directly. In addition, the choice of pump source should also consider issues such as excitation efficiency.

- Optical resonator

the amplification of the excited emission is not strong enough for most laser media. The part of the light wave that is amplified by the excited emission is often lost by other factors in the medium (absorption by impurities, scattering). So that the excited emission cannot become dominant in the laser medium.

The role of the optical resonator is the device that can strengthen stimulated amplification in the laser medium. The optical resonator is composed of two mirrors: a fully reflective mirror (or one with a high reflection coefficient) and the other is a partially reflective mirror. The optical axis of the resonator is aligned with the long axis of the laser medium. Thus, the light waves that propagate along the resonator axis will be reflected back and forth between the two reflective mirrors. The light repeatedly passes through the laser medium many times. In this way, the light is constantly amplified. The light waves propagating along with the other directions quickly leak out of the cavity. Resonator makes the light waves that only propagating along the cavity axis preferentially amplified. The resonator is the reason that light output from the optical resonator has excellent directionality.

The key condition for generating laser beams is population inversion between the high and low energy levels. In general, the excited emission is very weak and even negligible, so it is difficult to produce laser light. Assume that the population on the low energy level E_1 is N1 and the population on the high energy level E_2 is N2. When the laser medium is in thermal equilibrium, the distribution on the energy level follows the Boltzmann distribution. When a system is in thermal equilibrium, a lower-lying level is more strongly populated than higher-lying energy. The pump source activates the laser medium to disturb the distribution of energy levels in the atom. The laser medium is in a state of population inversion: N2>N1.Figure 2.1.5 [15] shows the normal population and population inversion.

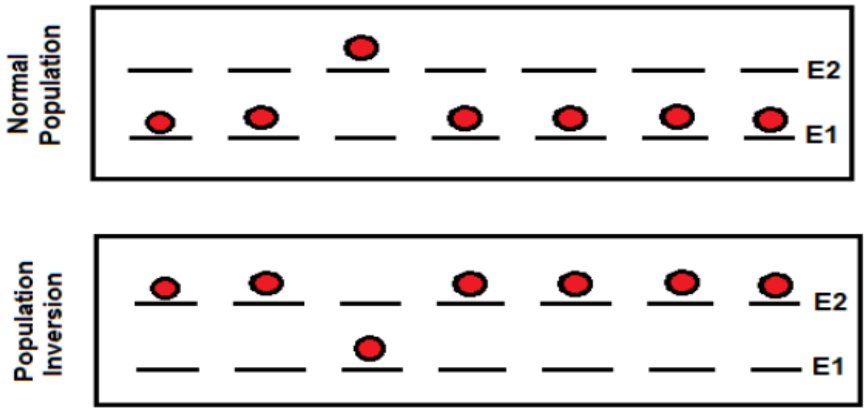

Figure 2.1.5 Normal population and population inversion.

2.2 Lasers used in the experiments

2.2.1 The spectrum in laser

Two lasers with different light sources will be used in the following experiments: green laser and infrared laser. The wavelength of the laser can classify the type of laser.

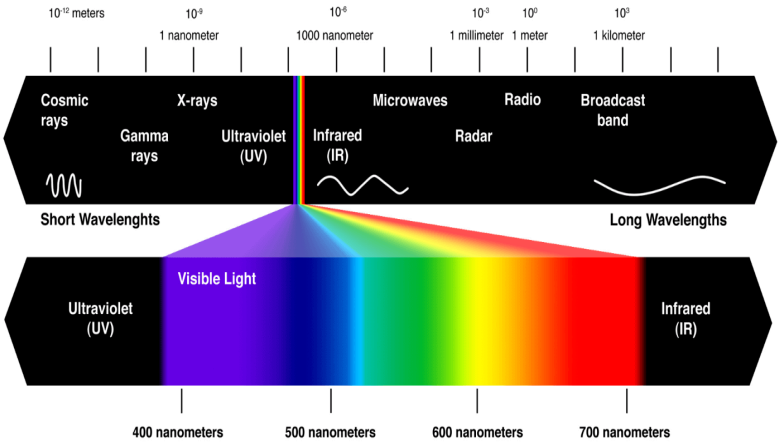

Figure 2.2.1 The spectrum of light.

The light spectrum shown in figure 2.2.1 [16] is the many different wavelengths of energy produced by a light source. The light can be divided into different types according to wavelength (or frequency), for example, infrared light, visible light, and ultraviolet light.

Generally speaking, infrared is an electromagnetic wave with a wavelength between microwave and visible light. Infrared light means light with a wavelength between 760 nm and 1 mm. It is an invisible light with a longer wavelength than red light. The corresponding frequency is about 430 THz to 300 GHz, which is the part of the electromagnetic spectrum that the human eye can recognise. The visible spectrum has no precise range; the frequency of electromagnetic waves that most eyes can perceive is between 380 and 750 THz, and the wavelength is between 780 and 400 nm. The electromagnetic waves with wavelengths between 10nm and 400nm are called ultraviolet rays. Ultraviolet wavelengths are shorter than visible light but longer than X-rays.

It covers all kinds of lasers from X-ray to far-infrared in the order of wavelength from short to long, and the wavelength ranges from 0.001 nanometers to 1000 micrometers. Among them, the laser directly output by the fibre laser is mainly in the near-infrared part. However, to achieve different application needs, fibre lasers can output visible light through frequency doubling.

2.2.2 The Infrared (IR) Lasers

The IR laser in figure 2.2.2 [17]was used to cut and anneal the wafer in the following tests. The laser source SP-050-P-A-H-S-S comes from SPI laser limited.

Figure 2.2.2 50W HS-S laser source

Some critical parameters are indicated in the table2.2.1 [17].

Parameter	Unit	SP-050P-A-HS-S
Central emission wavelength	nm	1059 - 1065
Nominal average output power	W	50
M^2		<1.3
Collimated beam diameter	mm	3 / 5 / 7.5 / 10
PulseTune waveforms		24
Maximum pulse energy	mJ	>0.7
Maximum peak power	kW	>7
Pulse duration range	ns	11 - 220
Pulse repetition frequency (PRF) range	kHz	1 - 1000
CW mode (with modulation)	kHz	YES (1 - 100)

Table 2.2.1 Specification of IR laser

As a pulsed laser, the pulse shape under ideal conditions is a standard Gaussian distribution. However, a laser generator cannot produce a perfect Gaussian distribution in practice, leading to many different waveforms selected in practical applications. Fix the output waveform of the infrared laser at waveform 0, which means that the maximum output power can always be obtained. The comparison between different waveforms can refer to in figure 2.2.3 below. When the output waveform 0 is selected, the frequency becomes the critical factor affecting the pulse. It can be seen from figure 2.2.3 that when the frequency continues to increase, the maximum power of the pulse will correspondingly decrease. It is recommended to use frequencies of 70 kHz and above for work. By the way, the pulse duration at 10% is 220 nanoseconds, and the maximum pulse energy reaches 0.71 mJ. An F-Theta objective focuses the deflected laser beam before it hits the surface of the product. Generally speaking, the processing is carried out within the focus of the beam. The f-Theta focal length is 160 mm.

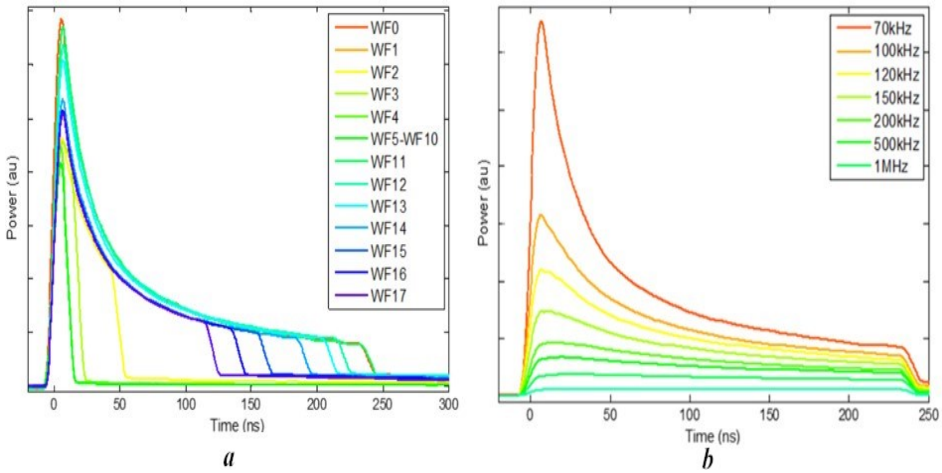

Figure 2.2.3 Waveform characteristics. a) Pulse Shapes for Waveform 0 to 17 at Respective PRF0. b) Pulse Shapes for Waveform 0 at Varying PRF

There is additional work to calibrate the output power of the laser. Since the output power on the panel is current, it is necessary to convert it into power. The current can be set to any value from 0 A to 100 A in the software. However, it is not possible to calculate the output power of the laser with the current only through a simple proportional relationship. Multiple measurements are made using a power meter, and the results are fitted to find the relationship between current and output power.

The output power with tested current value from 10 A to 100 A increases the current by 10 A each time. Fix the output frequency of the laser at 70 kHz.The measured values can be seen in Table 2.2.2 below.

Current(A)	Power(W)
10	1.4
20	6.5
30	11.4
40	16.3
50	21.2
60	26.2
70	31.1
80	36.3
90	41.3
100	46.6

Table 2.2.2 Measured output power

The current setting value ranges from 10A to 100A, with an increase of 10A each time.

It shows that the maximum output power of this IR laser is 46.6 watts instead of 50 watts. After that, the figure between the current and output power can be plotted.

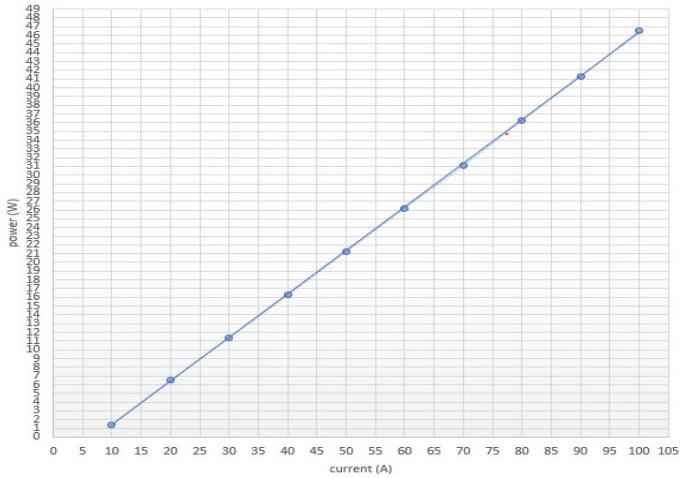

Figure 2.2.4 Fitting curve of current and output power

The relationship between the current and work output rate can be expressed as:

$$P=0.4996I-3.6476 \quad (2.1.2)$$

P with units watt represents the actual output power of the laser. I with units ampere represents the current value set in the software.

The beam divergence and the beam spot size are also crucial for lasers. Beam divergence is an angular measure of the beam diameter or radius increase with distance from the optical aperture or antenna aperture from which the beam emerges [18]. Beam Diameter is defined as the distance across the centre of the beam for which the irradiance equals $\frac{1}{e^2}$ of the maximum irradiance. The spot size of the beam is the radial distance from the centre of maximum irradiance to the $\frac{1}{e^2}$ points. For this infrared laser, beam divergence is 0.5 mrd. The laser beam spot size can be calculated with the following simple formula.

$$\emptyset_{spot}=f_{lens}\bullet\theta = 160mm \bullet 0.5mrad = 80um \quad (2.1.3)$$

The parameter f_{lens} is the f-Theta focal length and θ means beam divergence. The diameter of the spot is 0.08 mm, the area of the spot is 5.027×10^{-5} cm^2.

2.2.3 The green laser

Green lasers are ubiquitous in the industry. Generally, green lasers represent lasers with a wavelength of 532 nm to 556 nm. VLASE^{TM} GREEN is used in this experiment and has a wavelength of 532 nm. The characteristics of the green laser can be seen in table 2.2.3. It can be known from the table that the ideal maximum power of this green laser should be 10 watts. However, after the measurement of the power meter, the maximum power is 7 watts. Knowing the actual maximum power of the laser is very useful for subsequent work.

The laser produces a beam of high-energy invisible radiation. For more precise focusing, the laser beam is first magnified using an optical expansion system, then deflected by a scanning system made up of two mirrors mounted on galvanometer motors. The beam is deflected in a regulated beam along the X and Y axes by these mirrors. The product's surface is processed by the movement of two motors coordinated

with the on/off of the laser beam [19]. The f-Theta focal length for the green laser is 160 mm.

PERFORMANCE

LASER MARKER SOURCE (specification @ 25°C)		
Laser Type		Class 4 DPSSL (Diode Pumped Solid State Laser)
Average Power at reference Rep Rate (50kHz)[1]	W	10.0
Pulse energy (max)	mJ	0.35 (10ns)
Peak power (max)	kW	35
Central emission wavelength	nm	532
Repetition Rate[2]	kHz	20 ÷ 100
Laser aiming beam		Class 2 <1mW @ 630-670nm
Cooling		Forced Air Rack Fans = L10 @ 40°C : 60000h Resonator Fan = L10 @ 40°C : 70000h
Noise	dB(A)	< 70 at 1 meter

OTHER		
Optical Fiber Minimum Bending Radius	mm	200 (fixed installation)
Cables Length	m	3 standard, other available
Marking Speed	mm/s	Up to 3000 mm/s
Char Marking Speed[3]	char/s	Up to 360 char/s
MOF (Marking on the fly)		YES [constant speed or encoder]
Line speed ¯ Productivity[4]		Up to 75 m/min – 3 Pcs/s
Marking Control and Software		EMC Embedded Control and Lighter Suite
Communication		RS232, Ethernet (TCP/IP 10, 100 Mbit), digital I/O

Table 2.2.3 Specification of Green laser

Similarly, the spot size of the green laser can be calculated. However, unlike the infrared laser, the beam divergence of the green laser is 0.8 mrad.

$$\varnothing_{spot}=f_{lens}\bullet\theta=160mm\bullet 0.8mrad=128um \tag{2.1.4}$$

The parameter f_{lens} is the f-Theta focal length and θ means beam divergence. The diameter of the spot is 0.128 mm, the area of the spot is 1.287×10^{-4} cm^2. The spot size above is only a calculated theoretical value. The precise laser beam spot size should be obtained using laser beam profilers.

Chapter 3 Laser cutting wafer

Wafer cutting(or wafer dicing) separates the die from a semiconductor wafer. Following the dicing process, the individual silicon dies are encapsulated into chip carriers suitable for building electronic devices such as computers.

3.1 Method of wafer cutting

Wafer cutting dates back to approximately 1955, with the earliest format being diamond scribing and breaking, followed by laser [20]. Wafer cutting is generally carried out using conventional blade technology. Scribing and breaking, mechanical sawing (usually with a dicing saw), and laser cutting are all options for dicing. In order to guarantee precision and accuracy during the production process, all processes are usually automated. By selectively processing all technical ceramics and silicon, laser cutting opens up new possibilities [21]. There is no mechanical cutting force or tool wear involved.

- Cut by the dicing saw

In a dicing machine, the mechanical dicing operation is carried out using the full cut dicing method. A series of preparations are required before cutting. A dicing tape with a base film and an adhesive layer on top is used to fix the wafer on a dicing frame. The dicing blade, which acts as the primary cutting tool, is mounted in the spindle of the dicing equipment. The dicing blade has synthetic diamond particles embedded in a suitable medium. When a worn-out particle falls out during the dicing operation, it exposes a new diamond particle. The wafer placed in the wafer frame held in a vacuum chuck travel at a specified feed rate passing through the dicing blade in X and Y directions for device singulation, and the dicing blade spins at 30 to 50K rpm [22].

Depending on the capabilities of the dicing equipment, several types of dicing cut methods are possible. Common methods in practice are single cut, dual-pass, and step cut. The traditional cutting dies method utilises one blade, and one spindle in a single pass is known as a single cut. Dual pass refers to cutting the chip with one blade mounted on a spindle but the same blade travelling through the same saw street twice, each at a predetermined depth of cut. Step cutting is the process of cutting a die utilising

two blades positioned in two spindles (commonly referred to as dual spindle) that spin at the same or different rpms.

The key parameters include spindle (blade) speed in rpm, feed rate in mm/sec, and cut depth, among the dicing process parameters (depending on different dicing cut methods). Silicon cutting requires an optimal cutting force to break the internal crystallographic connections that arise from the enhanced process parameters stated above [23]. Cutting forces that are too high or too low will result in dicing defects such as poor chipping or dicing blade failure. The dicing parameters are influenced by the amount of material removed by the blade and the diamond grit size, concentration, and blade bond type [24].

The dicing saw method is limited by blade lifetime, width, chipping and delamination, and slow feed speeds. In addition, when cutting other substrates, the dicing saw method introduces other new problems. For example, glass is often used in high-frequency communication equipment because of its resistivity characteristics. In addition, according to different needs, silicon carbide and sapphire can replace silicon as a substrate. It is challenging to dice with traditional blade sawing because of their hardness and chemical inertness [25].

- Cut by laser

The industry is moving toward alternative separation methods due to the recent tendency [26] to lower substrate thickness. The mechanical stresses of the blade dicing process make thinner wafer cutting complex [27]. The semiconductor industry is still looking for a low-cost separation solution that delivers excellent yield and productivity. Laser cutting means wafer dicing process by laser ablation, in which material is removed by evaporation and melt ejection under the irradiation of laser pulses. Ablative laser dicing has been studied extensively, primarily on blank silicon wafers.

Laser cutting is becoming more and more important in modern technology. Because it is contactless, the laser alternative for wafer cutting requires fewer consumables, can be precisely focused and is predicted to produce less chipping and delamination. Different lasers have different characteristics (wavelength, pulse duration, beam shape), and different materials have different properties (mechanical, optical, and thermal). Only when the laser and the material are matched can the result be optimised. The same laser is difficult to fit all materials. Laser cutting wafers can be done in

various ways: including laser scribe-break [28], stealth dicing, water jet cooling, multi-laser beam technique, and filament cutting.

Laser scribe-break is the most straightforward approach, and it is currently used in manufacturing plants. All of the steps are automated and take place in a white room condition (A white room is another type of controlled environment typically used to produce precision mechanisms and medical devices). A sticky tape is frequently combined with a ring or frame in the microelectronics sector (usually 12 inches diameter). After that, the wafer (typically 6 inches in diameter) adheres to the tape. The frames are contained in "cassettes" and are controlled by robotic arms. This makes wafer handling easier, avoids touch, and retains the diced chips on support. During the scribing process, the laser beam travels through the wafer. The depth of the groove should be between a quarter and a third of the wafer thickness. It is necessary to clean the wafers and frames before and after laser dicing. The frame and wafer are taken to a breaking machine. A blade is positioned beneath the tape/wafer while the frame is maintained. Two "shoes" then push down on the wafer, breaking it along the groove carved by the laser beam earlier. As a result, the dies are separated.

The "Water jet cooling" technique combines a water jet with a laser beam. Water jet-guided laser processing based on total reflection can perform better than the conventional cutting method [29]. The nozzle produces a consistent low-pressure water jet that functions as a waveguide for the laser beam, similar to an optical fiber. The laser beam's penetration depth generally restricts ablation in traditional laser machining. Other factors, such as the accumulation of debris inside the groove, also limit the cutting depth (laser loss caused by multiple reflections). The water jet cleans the groove while also increasing the cutting depth. On the other hand, a low-pressure water jet can ensure that the substrate material is not damaged. The constantly flowing water can cool the substrate, reducing local overheating and limiting the generation of debris and cracks [25].

When using a laser to cut more rigid materials such as sapphire and silicon wafers, the scanning speed of the laser needs to be reduced. Of course, a multi-laser beam process is also a good choice. The multiple laser beam dicing technologies are a derivative of the line-shaped beam dicing approach [30]. The main idea is to divide the laser light into several laser beams after passing through the diffractive optical elements

(DOE) [31]. According to research, ALSI® (Advanced Laser Separation International) has divided the laser light into up to 48 parallel low-energy lasers through diffraction. The distance between parallel laser beams ranges from 10 μm to 1000 μm [32]. The principle can be seen in figure 3.1.1 [33]. With multiple laser beams aligned in parallel, multiple grooves can be drawn on a wafer simultaneously.

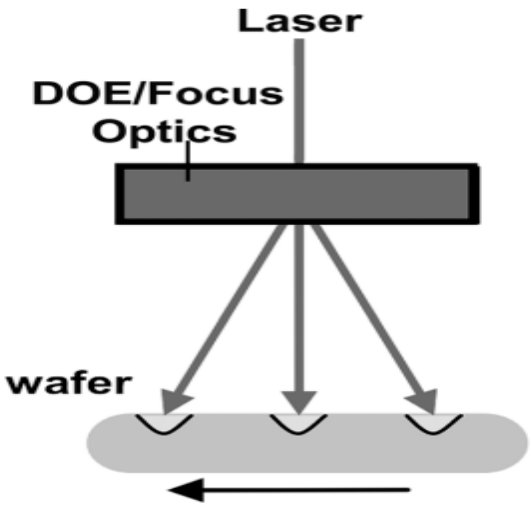

Figure 3.1.1 Multi-beam laser structure.

Stealth dicing was developed and commercialised by Hamamatsu Photonics ®. Unlike conventional blade dicing, stealth dicing engines cut the material from the inside by concentrating a laser beam on an interior location of the material to be diced. A limited area around the light's focal point results in mechanical damage or stress layer [33] [34].

Generally, two different mechanisms are used when laser cutting wafers, namely laser ablation and laser-breaking. The laser beam is focused on the surface of the wafer, and the laser beam's energy is absorbed. The absorbed energy will cause the surface of the wafer in contact with the laser beam to be ablated or even fractured. Contaminants are inevitably produced in the laser ablation method. The scorched particles are adsorbed on the surface of the wafer and are difficult to remove. In the laser-breaking method, in order to separate the dies from the wafer, cracks have to be made on the surface of the wafer, but the crack propagation, on the other hand, does not necessarily follow the desired cracking line. Stealth dicing has advantages over blade cutting and has better performance than general laser cutting. The approach is entirely distinct from previous laser-based technologies. One of the most important distinctions is that laser

processing happens exclusively on the interior of the wafer. The SD technique allows dry processing for no debris contaminants formed on the wafer surface.

The basic principle of laser stealth dicing is shown in figure 3.1.2. A designed laser beam passes through the surface of the target wafer and focuses on the interior of the wafer. The plane focused inside the wafer is called the SD layer [35]. A laser beam passes through the surface of the target wafer and focuses on the inside of the wafer. The plane focused inside the wafer is called the SD layer. When the wafer and the laser move relatively, the SD layer inside the wafer changes properties, thus completing the Stealth dicing.

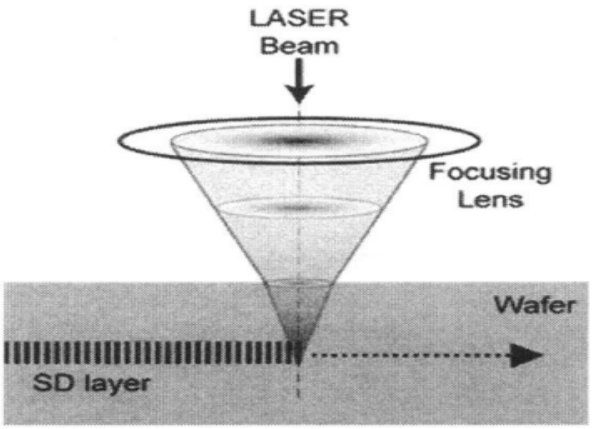

Figure 3.1.2 Schematic of stealth dicing

3.2 Wafer preparation

The 6" silicon wafers are used for the cutting and annealing process. It is an n-type wafer with a thickness of 400 um, which is fabricated by the FZ method and polished on both sides. The doped impurities are phosphorus atoms, once heavily doped and once lightly doped. The doping concentrations are 7E14 (at/cm2) at 60 Kev and 3E13 (at/cm2) at 60 Kev.

It is required to make dies with the dimension of 1.27 cm x 1.27 cm(a square with sides 0.5 inches long). In theory, an entire six-inch wafer can be cut into 52 dies. See figure 3.2.1 for more details.

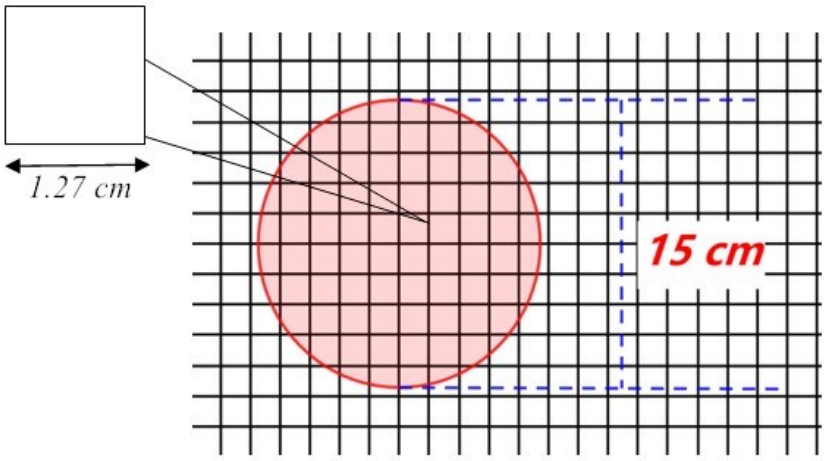

Figure 3.2.1 Schematic of the wafer and small die

It is necessary to apply the photoresist to protect the wafer from the slag generated during cutting. Photoresist only plays the role of a protector, which has nothing to do with photolithography. Before cutting, use *POSITIV 20* from *KONTAKT CHEMIE*, a liquid photo-positive resist photoresist. After spraying the photoresist on the clean wafer surface, place it in a 70 ℃ oven for 15 minutes, or place the wafer at room temperature for 24 hours. When the photoresist is completely dried on the surface, a smooth and bright protective coating will be formed on the surface of the wafer.

For removing the photoresist coating, acetone or other ketone solvents can be used. Put the acetone solvent into the beaker and the beaker into the ultrasonic cleaner, which a small amount of water already exists. Adjust the power of the ultrasonic cleaner to the maximum, set the temperature at 50 ℃, and set the cleaning time to five minutes.

3.3 Infrared laser cutting wafer

There are two ways to cut wafers, cutting from the front surface and cutting from the back surface. Both cutting methods need to spray photoresist on the front surface of the wafer to ensure the cleanliness of the wafer surface.

The key parameters that need to be adjusted when cutting wafers with infrared lasers are current (power), pulse frequency, scanning speed, number of scribe lines, and pulse width. For each test, the edges of the wafer being cut should be observed under a microscope to determine if the parameters are as expected. When the defect area on the edge of the silicon die after being cut is smaller, the actual available area of the silicon die is larger, and the cutting effect is better.

After three tests cut from the front side of the wafer, then analyze the results obtained. Observe the obtained results under a microscope, and use software to measure the range of edge defects. To ensure the accuracy of the results and eliminate random errors, each sample is measured three times at the edge, and then the mean value is calculated.

NO.	MARK TIMES	MARK SPEED(mm/s)	CURRENT(A)	FREQUENCY (KHZ)	PULSE WIDITH(us)	DEFECT 1(μm)	DEFECT 2(μm)	DEFECT 3(μm)	Mean Defect(μm)
1	30	1000	33	75	33	56.48	17.83	26.74	33.68
2	30	1000	38	75	33	60.67	59.43	52.24	57.45
3	30	1000	40	75	33	38.26	24.89	24.14	29.10

Table 3.3.1 Three sets for cutting test.

The laser mark times, pulse frequency, pulse width, and marking speed are all the same for the three sets of tests. The main difference between them is that the output energy of the pulsed laser, where the energy is expressed in the form of electric current. The results of the three sets of tests under the microscope are shown in figure 3.3.1.

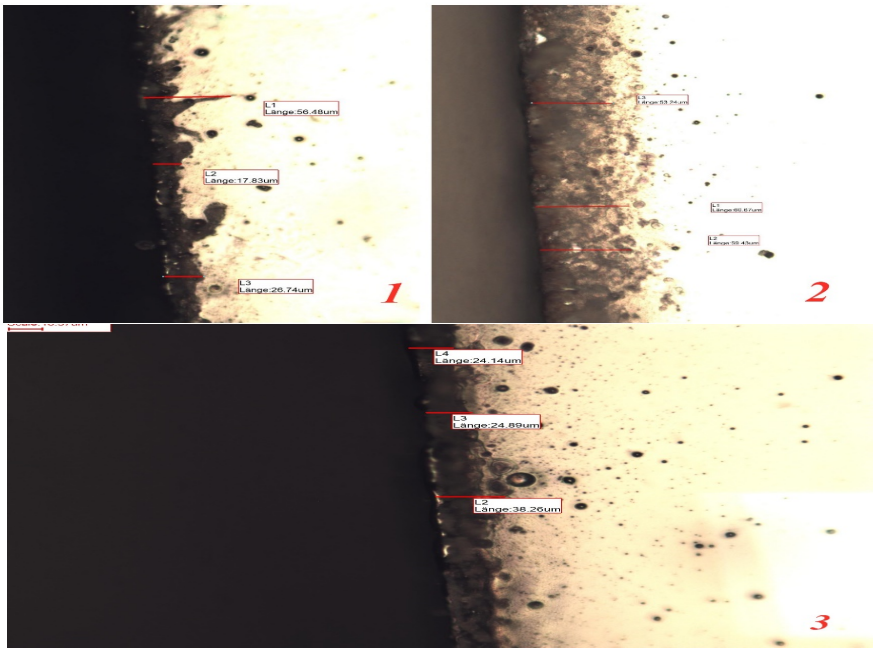

Figure 3.3.1 Microscopic view of the cut silicon edge

Calculating the laser output power under the three sets of currents use the calibration equation, the power can be known as 12.85 watts, 15.34 watts, and 16.34 watts at 33 A, 38 A, and 40 A, respectively. From the BeamGage® analysis, it can be inferred that the central area of the Gaussian with a diameter of 0.02 mm contains about 15% of the total power. The actual laser beam spot area is 3.14×10^{-4} cm^2. Therefore, it can be calculated that the actual power received on the surface of the silicon wafer in the three sets of tests is 1.928 watts, 2.301 watts, and 2.451 watts, respectively.

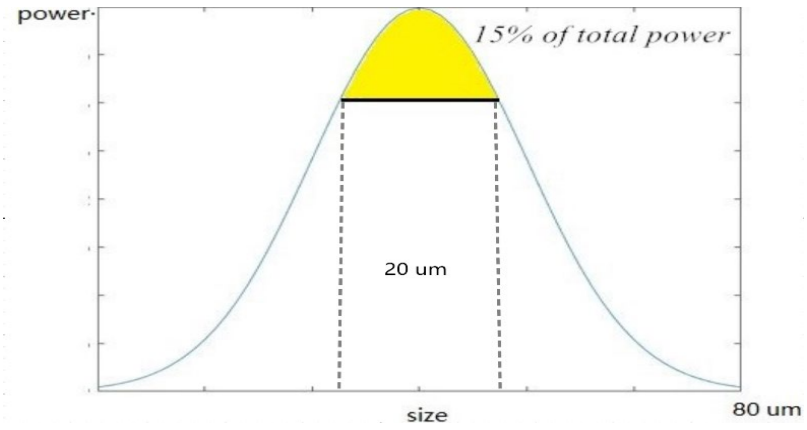

Figure 3.3.2 Gaussian distribution with 15% useful energy

Further, calculate the pulse energy and fluence (per pulse). For the above three sets of tests, their pulse energy is 0.026 mJ, 0.031 mJ, and 0.033 mJ. Their fluence is 8.28 J/cm^2, 9.87 J/cm^2 and 10.50 J/cm^2 respectively.

$$\text{Pulse energy} = \frac{\text{Average power}}{\text{Frequency}} \tag{3.1.1}$$

$$Fluence = \frac{\text{Pulse energy}}{\text{Area}} \tag{3.1.2}$$

It is much easier when using a laser to cut from the back surface of the wafer. When cutting on the backside, minor edge defects will be left on the front side of the wafer so that a larger laser power can be used. High-power output means that the mark times can be reduced, thereby increasing the cutting speed. It should be noted that when a higher power laser is applied to the back of the wafer, the front of the wafer may be contaminated by slag. There are two solutions to this problem. Before laser cutting, the photoresist is still sprayed on the surface of the wafer. During the laser cutting process, the photoresist can protect the front surface of the wafer from high-speed and high-

temperature slag damage. After the cutting is completed, the slag on the small die surface and the film formed by the photoresist is washed away with an acetone solvent in an ultrasonic cleaner. After that, if there are still contaminants on the front side of the wafer under the microscope, it can be cleaned with lens cleaning paper. Press the lens cleaning paper gently on the surface of the wafer, and then slowly wipe the surface of the wafer in one direction at all times.

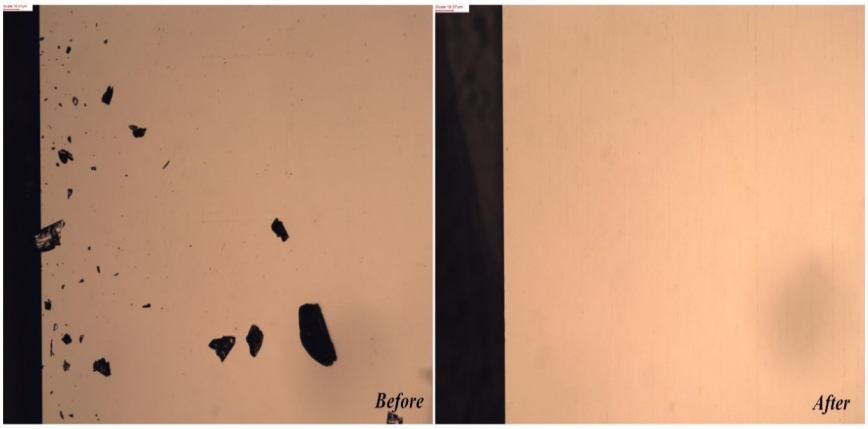

Figure 3.3.3 Results after cutting on the back side under the microscope

The comparison before and after wafer cleaning is shown here. At this time, the wafer cutting conditions are set to the output current of 50 A, output power of 21.34 watts, pulse frequency of 70 kHz, and marking times of 10. Consider that the actual power acting on the wafer surface is 3.2 watts. The pulse energy is 0.046 mJ, and fluence is 14.64 J/cm^2. At the same time, the marked speed can also be increased to 2000mm/s. The high output power of the laser has been increased, and the cutting speed has also been faster. The results obtained from the optical microscope show that the edges of the silicon wafer are almost free of defects. Contaminants that the ultrasonic cleaner cannot remove can be wiped away with optical lens paper

It can be inferred that increasing the output power of the laser within a certain range can deepen the cutting depth of the wafer and reduce the edge failure area. Similarly, increasing the scanning speed will also enable the laser to cut the wafer deeper. Because increasing the scanning speed of the laser means that the laser overlap in the cutting direction of the wafer is increased. Especially when the laser beam is used to cut from the back surface, the defect problem of the silicon wafer along the cut can be solved well.

Chapter 4 Laser annealing

An infrared laser and a green laser will be used to anneal the dies cut from the wafers. Then a microscope, profiler, and Raman spectroscopy will be used to compare and analyse the laser-treated silicon dies.

4.1 Theory of laser annealing

Compared with traditional annealing methods, electron beams and lasers can complete the annealing process of doped wafers faster. In addition, the electron beam and the laser can be controlled manually. The operating space and temperature can be manipulated so that the wafer can be heated locally. Electron beam annealing requires a vacuum or inert gas conditions, but lasers do not require these conditions, so lasers are more suitable for wide applications in industry.

According to the literature [36], laser annealing technology was first proposed in 1975. The former Soviet scientist Gerasimenko and his collaborators made a conference report in 1975. They observed that the structural damage caused by ion implantation in the silicon crystal after laser irradiation was effectively eliminated, and the electrical properties of the sample doped layer were significantly improved.

The laser annealing process is a top-down heating process. When the laser irradiates the material's surface, the temperature on the material's surface is the highest, and there is a temperature gradient inside the material. The shorter the time it takes for the temperature to rise and the greater the temperature gradient, the slower the impurities within the material will diffuse to the surface. Different types of pulsed and continuous (CW) lasers may recrystallize disordered silicon through different processes. Because regrowth of the crystal lattice occurs in the solid phase, CW laser annealing is comparable to the traditional furnace method [37]. When the laser beam is swept over the sample, there is little time for the dopant to diffuse into the bulk of the wafer; the high temperatures are only sustained for milliseconds. Compared with furnace treatment, CW laser annealing effectively eliminates extended structural defects (such as stacking faults and dislocations) and deposits more dopants at electroactive substitution sites. A distinctive feature of pulsed laser annealing is that high energy density laser irradiation is projected over a small area of the annealed sample in a very short time. The laser light melts the material on the surface of the sample. The growth

of the crystal film is then naturally extended beyond the liquid phase of the melted layer, reconstructing the crystal structure of the melted layer. During this process, the impurity atoms migrate farther [38]. Then the impurity atoms are embedded in the crystal structure, thereby being activated to release holes or electrons.

In the subsequent more systematic research on the annealing mechanism, scientists found more conclusions [39].

Laser annealing can significantly remove lattice damage.TEM and Rutherford backscattering to study the sample lattice damage after laser annealing shows that laser annealing can more effectively eliminate dislocations and lattice damage and maintain the lattice arrangement.

Laser annealing can change the dopant profile. Secondary ion scattering shows that the distribution of impurity ions before and after annealing has changed significantly. The researchers further demonstrated that the melting of the material accompanies the process of laser annealing.

After laser annealing, the crystal lattice of the region where the ions are injected has undergone a significant change. The Bragg reflection test was performed on the silicon wafer before and after annealing. The results show that the lattice in the ion implantation region shrinks or expands in the one-dimensional direction after annealing. Ions Back-scattering shows that impurity ions injected into the crystal lattice can fill the lattice vacancies. The concentration of impurity ions in the crystal lattice can far exceed the limits of solid solubility.

4.2 Preparation before annealing

Use the samples cut by laser to perform annealing experiments. It is required to make samples with the dimension of 1.27 cm x 1.27 cm(a square with sides 0.5 inches long). Each sample is divided into two areas, only one area is subjected to pulse laser annealing treatment, and the other blank area is used for comparison with the annealed area.

The sample schematic is as figure 4.2.1. In the figure, the black part of the sample is the laser annealing area, and the white part is the untreated area, which is used for comparison. The N in the upper left corner represents the test number. Set the annealing area to be a rectangle with a size of 0.5 cm×1 cm.

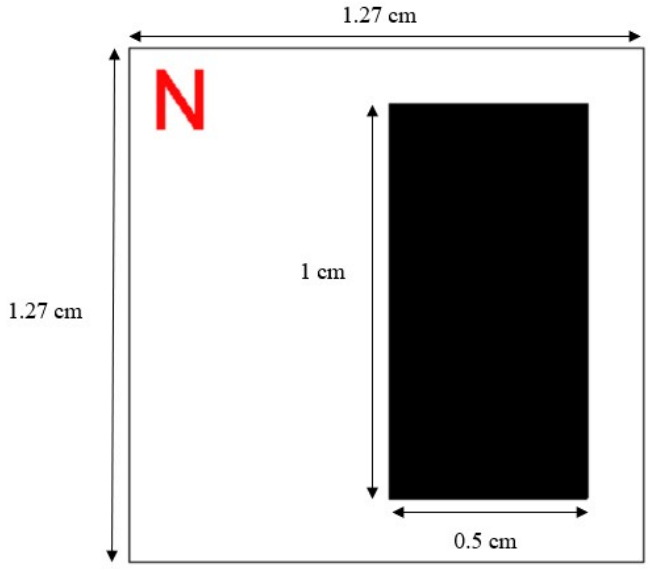

Figure 4.2.1 Schematic diagram of sample design

The action time of the pulsed laser on the surface of the wafer will also significantly affect the annealing effect of the wafer. Therefore, it is necessary to consider and calculate the dwell time of the pulsed laser in the annealing test. At the same time, the overlap of pulsed lasers should also be taken into consideration.

4.3 Additional parameters

4.3.1 Laser dwell

Dwell time can be used to characterize the length of time the laser acts on the material's surface. The longer the dwell time will cause the laser to affect deeper inside the material. Considering the different working methods of continuous laser and pulsed laser, the calculation method of dwell time is also different for these two types of lasers.

Dwell time can be intuitively interpreted as the duration of laser "stay" on a pixel. When the continuous wave laser is working, the power is continuously output and does not involve parameters such as frequency. Therefore, only the spot size and the scanning speed of the laser need to be considered when calculating the dwell time. According to the theory [40], the dwell of continuous wave can be expressed as

$$T_{dwell} = \frac{d_{spot}}{v_{laser}} \tag{4.1.1}$$

In equation 3.1.3, d_{spot} means the diameter of the beam spot, and v_{laser} is scanning speed. When considering the dwell time of pulsed lasers, it is necessary to pay attention to the characteristics of pulsed lasers. Pulsed lasers cannot continuously output energy like continuous-wave lasers. Pulsed lasers always work at the set frequency and pulse width. Therefore, the laser's working frequency and pulse width should be considered when calculating the dwell time. Make the dwell time expression of the continuous-wave laser a reference, and from a physical point of view, the dwell time expression of the pulsed laser can be derived.

$$T_{dwell} = \frac{f * \tau * d_{spot}}{v_{laser}} \tag{4.1.2}$$

In the equation, f is the frequency of pulse laser, which means how many pulses repetitions in 1 second and τ the pulse width. The physical meaning of f*τ is the ratio between "time of laser turn on" and the whole period. Furthermore, it can be verified that the dimension of pulse laser dwell time is a time unit.

4.3.2 Overlap

When considering the overlap of the lasers, the overlap of the lasers in the scanning direction (pulse overlap) and the overlap between each scanning track (line overlap) should be considered simultaneously. A large overlap along the scanning direction of the laser will cause uneven power distribution of the laser on the wafer surface. However, if the edge overlap is too small or even non-existent, the laser will not be able to radiate completely on the wafer surface.

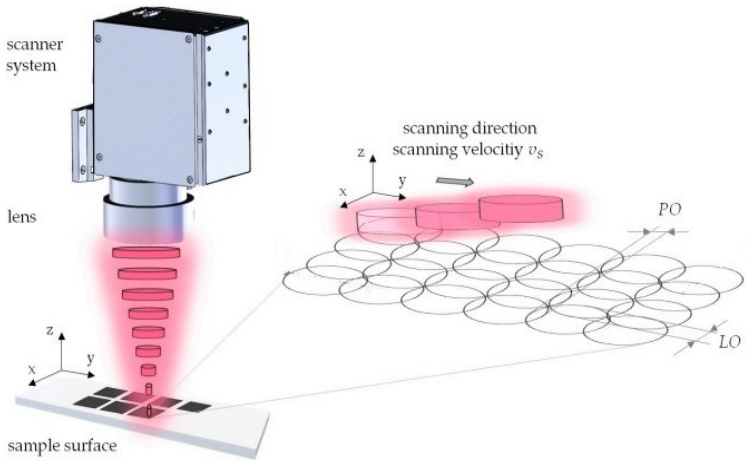

Figure 4.3.1 Overlap of the laser spot. Schematic illustration of the laser surface structuring using a line-wise scanning strategy leading to a defined laser pulse overlap (PO) and scanning line overlap (LO).

As shown in figure 4.3.1 [41], assuming that the scanning direction of the pulsed laser is from left to right, there will be overlaps of beam spots in the horizontal and vertical directions. The overlap in the vertical direction is also called line overlap. In order to Modify the pulse overlap, it is necessary to change the laser scanning speed and pulse repetition frequency. Pulse overlap can be expressed as:

$$PO = \frac{v_{laser}}{\mathrm{f}} \tag{4.1.3}$$

It can be known from the equation that reducing the scanning speed of the pulsed laser or increasing the repetition frequency of the pulse will reduce the pulse overlap.

Another parameter is introduced here, called interline hatching. Interline hatching means the distance between the center of one line and the center of the next line when the laser scans the surface of the material line by line. Interline hatching can be set on the laser control platform in the computer to change the line overlap on the surface of the material. The schematic is shown in figure 4.3.2.

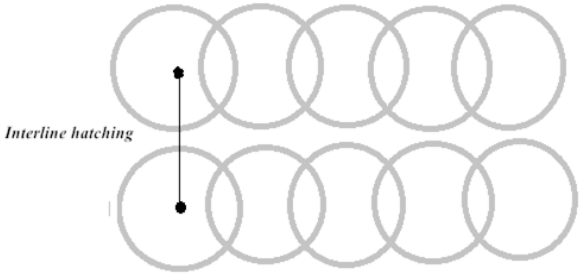

Figure 4.3.2 Schematic of interline hatching

4.4 Annealing with infrared laser

An infrared pulsed laser with a wavelength of 1064nm is used for annealing the silicon wafer. First, make a few samples. These samples are all made under the same conditions without gas assistance.

Put the annealed sample under the microscope for observation. Two features need to be observed under a microscope. First, make sure that the laser does not burn the surface of the silicon wafer. If the laser damages the silicon wafer, then the subsequent

tests will be meaningless. Secondly, it is necessary to make the laser uniformly act on the surface of the silicon wafer as far as possible so that there is no gap between each line after the laser is scanned line by line. In order to prevent the laser from damaging the surface of the silicon wafer, it is necessary to control the energy output of the laser. Strictly speaking, it is necessary to manipulate fluence within a reasonable range. On the other hand, by adjusting the interline hatching in the software, the spacing between the laser traces of each line can be changed. Too much power and large interline hatching bring negative results, as shown in figures 4.4.1 and figure 4.4.2.

.

Figure 4.4.1 Surface of silicon wafer damaged by laser. The outpower from the laser is 20w, and the fluence (per pulse) is 1.99 J/cm2.Too much power leads silicon atoms on the surface of the silicon wafer to be burned, then the surface is damaged.

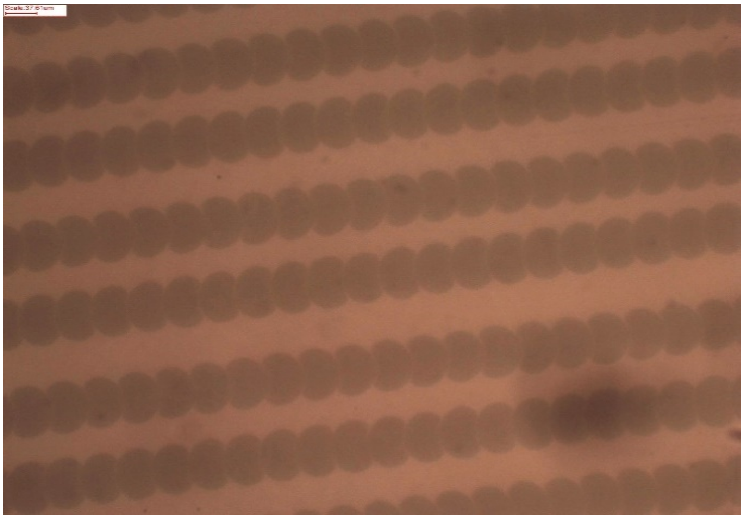

Figure 4.4.2 Incomplete wafer surface coverage by the beam spot. Interline hatching is too large for the laser to make a uniform trace on the silicon surface, and is no overlap between the laser lines.

According to previous estimates, it can be known that the beam spot diameter of this infrared laser is 20 μm. Therefore, when considering line overlap, the initial value of interline hatching can be set to 20 μm.

No.	Power [W]	Setted Power [W]	Pulse frequency [kHz]	Scan Speed [mm/s]	Interline Hatching [μm]	Pulse width [ns]	Area [cm^2]	Pulse energy [mJ]	Fluence (per pulse) J/cm^2	Peak power [kW]	Irradiance [MW/cm^2]	Laser Dwell [μs]	Overlap scan direction [μm]	current (A)
1	0.3	2.3	200	50	5	220	3.14E-06	1.725E-03	0.55	0.01	2.50	17.60	0.25	11.9
2	0.4	2.6	200	1000	7	220	3.14E-06	1.950E-03	0.62	0.01	2.82	0.88	5	12.5
3	0.4	2.75	200	1800	10	220	3.14E-06	2.063E-03	0.66	0.01	2.98	0.49	9	12.8
4	0.6	4.1	200	1800	20	220	3.14E-06	3.075E-03	0.98	0.01	4.45	0.49	9	15.5
5	0.68	4.5	200	1800	20	220	3.14E-06	3.375E-03	1.07	0.02	4.88	0.49	9	16.3
6	0.8	5.4	200	1800	20	220	3.14E-06	4.013E-03	1.28	0.02	5.81	0.49	9	18
7	0.9	5.9	200	1800	20	220	3.14E-06	4.388E-03	1.40	0.02	6.35	0.49	9	19

Table 4.4.1 Initial IR laser tests

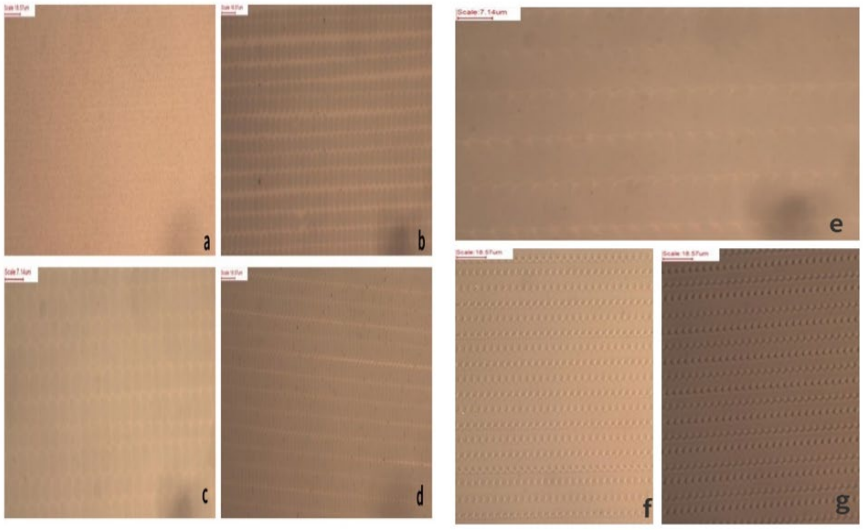

Figure 4.4.3 The initial IR samples under the microscope. The results of tests 1-7 observed under the microscope correspond to a)-g), respectively

As shown in table 4.4.1, the seven sets of tests continuously increase the actual output power of the laser and mean that the fluence of each pulse output is constantly increasing. In these tests, the effects of different interline hatching on the surface of the

silicon wafer were also compared. The results observed under the microscope can be seen in figure 4.4.3.

The results observed under the microscope showed that the surface of the silicon wafer after the seven sets of tests did not appear to be burnt by the pulsed laser. Moreover, there is a uniform laser spot track distribution, and the pulsed laser shows a good overlap when it acts on the surface of the silicon wafer. This means that for the silicon wafers surface, fluence from 0.55 J/cm^2 to 1.40 J/cm^2 is acceptable.

Roughness measurement is an important element of quality inspection in many industrial applications, including manufacturing and processing metals, semiconductors, ceramics, and plastics. Surface roughness can be determined using either electrical or optical methods. The mechanical profilometer is the most frequently used method for measuring surface roughness in manufacturing. It is well known that there are two different types of profile meters, namely, contact profile meters and non-contact profile meters.

Contact profilometer is also called probe profilometer. Probe profilometry needs force feedback and physical contact with the surface. Therefore, it is sensitive to soft surfaces, and the probe can become contaminated by the surface. Some surfaces may be damaged by this method. A probe profilometer is slower than non-contact methods because it requires physical motions in X, Y, and Z while keeping contact with the surface. The size and form of the probe tip might affect measurements and restrict resolution.

Light is usually used instead of probes in a non-contact profilometer. Non-contact profilometer can be accomplished in a variety of ways. The key to this approach is to direct the light to detect the surface in three dimensions.

Furthermore, in table 4.3.3 three samples are selected, and the roughness of the sample surface is checked by a probe profilometer which model is KLA Tencor P-15. The purpose of using the profilometer is to verify whether the pulsed laser has modified the surface of the silicon wafer. Renumber the three samples selected from the initial IR samples for profilometer analysis.

No.	Power [W]	Setted Power [W]	Pulse frequency [kHz]	Scan Speed [mm/s]	Interline Hatching [μm]	Pulse width [ns]	Area [cm^2]	Pulse energy [mJ]	Fluence (per pulse) J/cm^2	Peak power [kW]	Irradiance [MW/cm^2]	Laser Dwell [μs]	Overlap scan direction [μm]	current (A)
1	0.4	2.75	200	1800	10	220	3.14E-06	2.063E-03	0.66	0.01	2.98	0.49	9	12.8
2	0.68	4.5	200	1800	20	220	3.14E-06	3.375E-03	1.07	0.02	4.88	0.49	9	16.3
3	0.8	5.4	200	1800	20	220	3.14E-06	4.013E-03	1.28	0.02	5.81	0.49	9	18

Table 4.4.2 IR samples for profilometer

Complex settings on the profilometer must be performed before using the profilometer to check samples, such as the sampling speed and the force applied on the probe. Here, the sampling speed is 20 μm per second, and the force is 1 mg. When testing samples, to eliminate the influence of random errors, each sample is sampled twice. In the first sampling, the probe of the profiler scans the upper part of the sample from left to right. In the second sampling, the probe of the profiler scans the lower half of the sample from left to right. Figure 4.4.4 shows the details of twice samplings. The green arrow represents the direction of movement of the probe. It needs to be pointed out that it is necessary to ensure that the probe starts and stops scanning outside the annealed area.

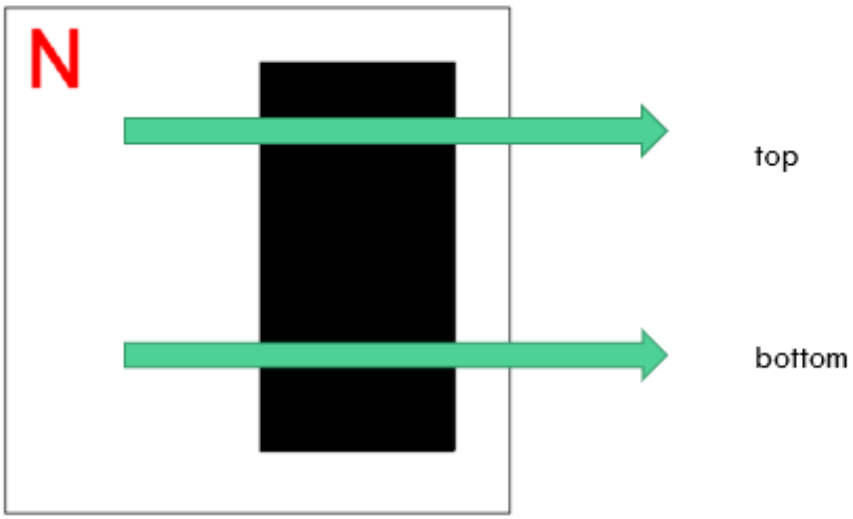

Figure 4.4.4 schematic of the sampling

P15 v7.0 User Manual [42]repointed the meaning of the parameters related to trace information of this profiler.

The result of sample 1 obtained from the profiler is shown in figure 4.4.5.

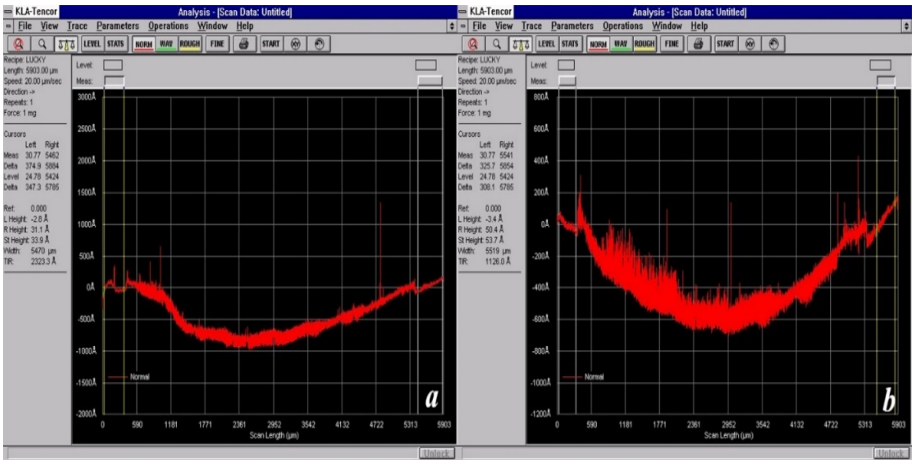

Figure 4.4.5 Profiler results for sample 1

The sampling length for sample 1 is 5903 µm. The left figure a) represents the probe scanning over the upper part of the silicon wafer, and b) in the right figure is the result of the probe scanning over the lower part of the silicon wafer.

Then observe the performance of the second annealed sample under the profiler. The result can be seen from figure 4.4.6.

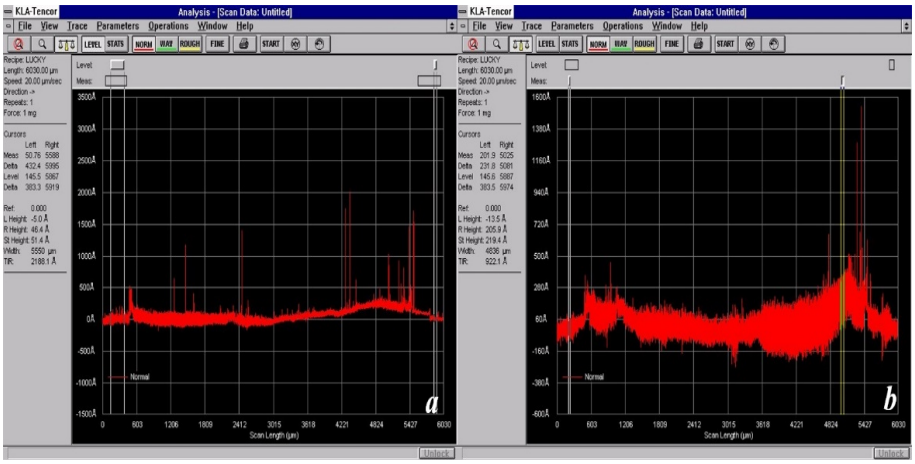

Figure 4.4.6 Profiler results for sample 2

For sample 2, the sampling length is 6030 µm, which is slightly longer than the sampling length of sample 1. Like sample 1, a) represents the result of sampling on the upper half of the silicon wafer, and b) represents the result of sampling on the lower half of the silicon wafer.

Finally, sample 3 is analyzed by the profiler. The result can be seen in figure 4.4.7.

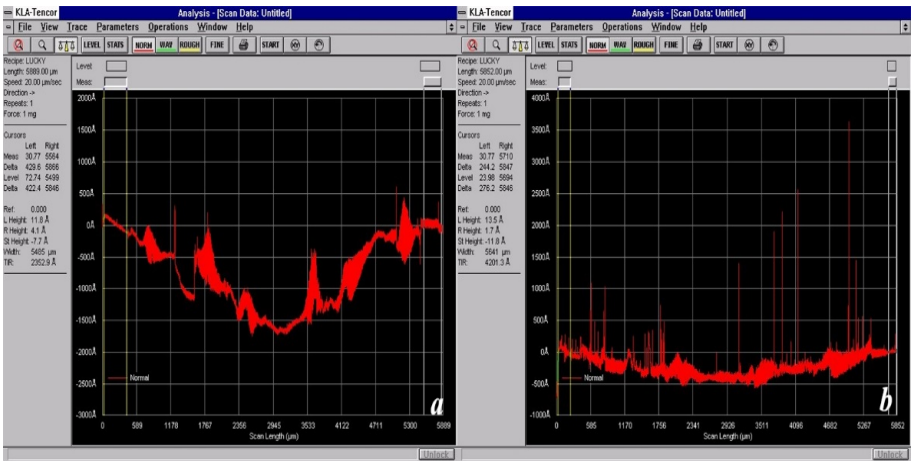

Figure 4.4.7 Profiler results for sample 3

The sampling length for sample 3 is 5889 µm. When the probe scans the upper part of the silicon wafer, the generated curve shows very obvious fluctuations, see a). This phenomenon may be because the upper part of the sample3 is heavily contaminated, or contaminants may appear on the probe's tip after multiple scans.

The above conclusions are only a qualitative analysis of the figures scanned by the profiler. It is impossible to know the exact roughness of the sample surface directly from the pictures. Only by relying on mathematical tools, the precise information can be obtained. The mathematical analysis of the data files obtained by the profiler can give quantitative conclusions.

Some important parameters can be used to evaluate the surface roughness of silicon wafers. The well-known central line average (CLA), also called arithmetic average height parameter (R_A), is widely used for manufacturing and scientific research roughness measures. R_A is defined as the average absolute deviation of the roughness irregularities from the mean line over one sampling length. Another commonly used parameter is the maximum height of the profile (R_{Max}), which is related to the profile's peak height and valley depth. R_{Max} is the distance between the highest peak and the lowest valley along the profile detection length [43].

The results of all scanning are shown in the table 4.4.3 below.

Sample	Region	Sampling Length(μm)	Sampling Points	R_{Max}(Å)	R_A(Å)
1	1 Upper	5903	14757	2323.31	432.44
1	1 Lower	5903	14757	1126.05	337.09
2	2 Upper	6030	15075	2188.13	87.20
2	2 Lower	6030	15075	2143.46	341.77
3	3 Upper	6889	14722	2352.87	740.07
3	3 Lower	5852	14630	4356.07	240.81

Table 4.4.3 Profiler results for IR laser samples

It is meaningless to focus only on the maximum roughness value of each scanning result because individual discontinuous spikes may be caused by contaminants, causing the probe to give incorrect feedback.

However, some conclusions can be drawn from the average roughness value of each group of tests. Among the six sets of tests performed on these three samples, the lower half of sample 3 showed the largest average roughness value, and its average roughness reached 740.07 angstroms. In the upper part of sample 2, the profiler analysis obtained the smallest average roughness of 87.20 angstroms.

Inspection of the annealed sample using a profilometer only allows the modification of the wafer surface by the pulsed laser to be observed. Raman scattering and Raman Spectroscopy are used to finding the solution to determine whether the pulsed laser has crystallized a wafer.

After discovering the Raman scattering effect in 1928, the study of the Raman effect has received widespread enthusiasm. Then a new technology-Raman spectroscopy analysis technology based on the Raman effect has gradually formed. Raman scattering is a phenomenon in which the frequency of outgoing light changes due to the interaction of incident light and molecules when light passes through a medium. From the Raman scattering spectrum, information about the molecular vibration and rotational energy level can be obtained. Since the specific vibration or rotational energy level corresponds to a specific chemical bond and molecular symmetry, the material species can be determined by Raman spectroscopy. The basis

of Raman scattering is inelastic scattering [44]. In some Raman spectra, the horizontal axis represents the wavenumber, while in other Raman spectra, the horizontal axis is Raman shift. The meaning of the two is the same, and they have the same unit $cm^{-1.}$

Researchers have obtained Raman analysis results of amorphous silicon and crystalline silicon through previous scientific experiments and drawn Raman spectra. The researchers found that in a typical Raman spectrum, the crystalline peak is located at about 520cm-1, and the amorphous silicon peak is about $470cm^{-1}$ [45], as shown in figure 4.4.8.

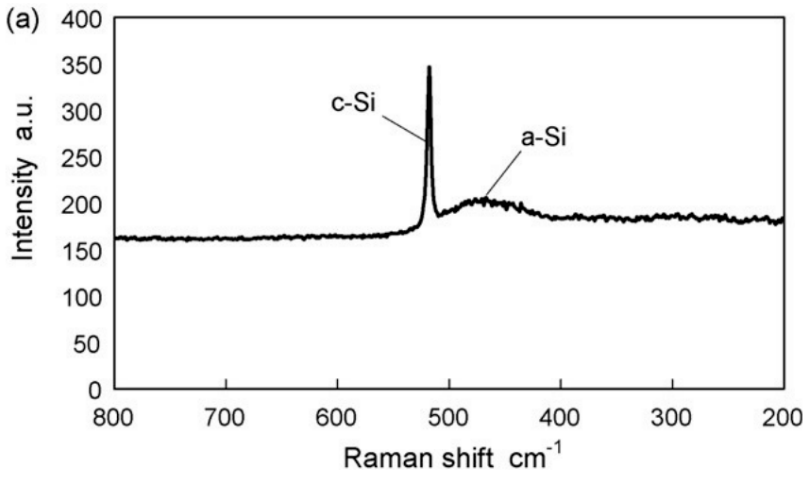

Figure 4.4.8 Raman spectra of amorphous silicon and crystalline silicon

Now go back to the samples in this experiment, perform Raman scattering on samples 1, 2, and 3 and generate Raman spectra. The wavelength of the laser source for Raman scattering is 514 nm, and two different incident laser powers are used to test each sample; the power of the incident laser is 1% and 10%, respectively. In particular, the Raman spectrum of the silicon wafer that the infrared pulse laser has not annealed is drawn.

Figure 4.4.9 shows the Raman spectrum of the non-annealed region of sample 2.

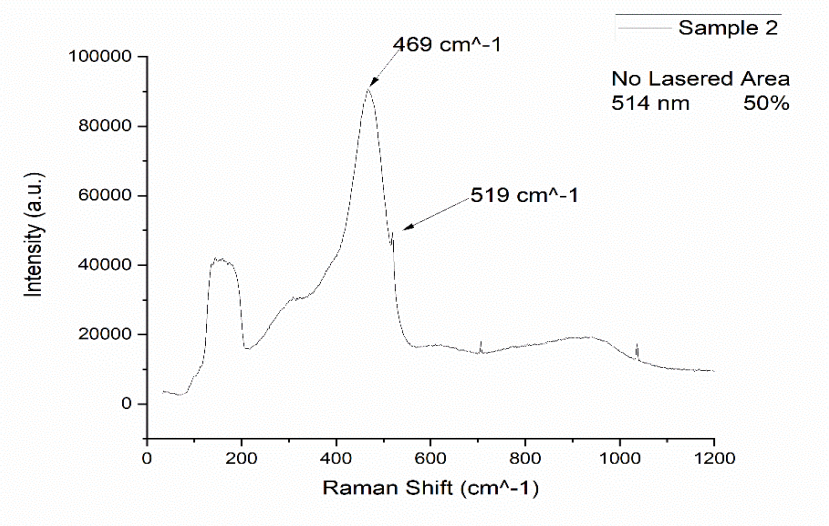

Figure 4.4.9 Raman spectra for the non-annealed region of sample 2

When the Raman shift appears near 470 cm^{-1}, this indicates that the area without annealing by the infrared pulse laser is still amorphous silicon, which is as expected. Then the 514nm laser with a power of 1% and 10% performs Raman scattering on all samples and obtains the Raman spectrum.

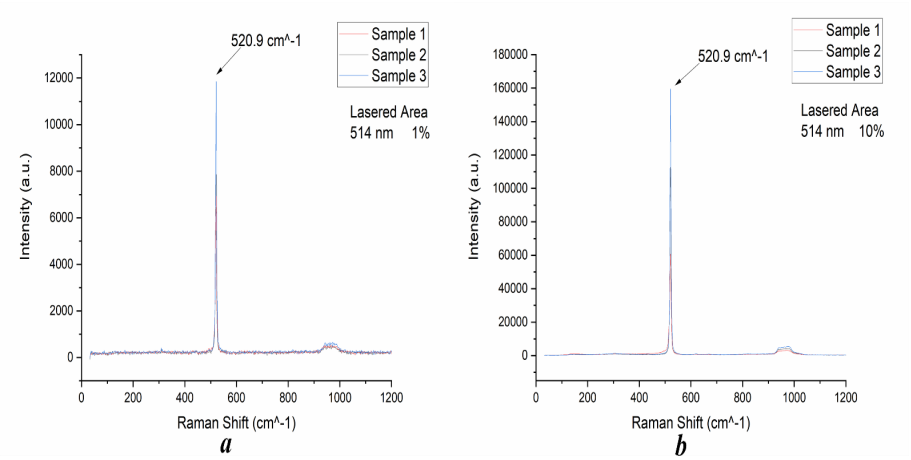

Figure 4.4.10 Raman spectrum for annealed region of IR samples

In figure 4.4.10, a) is the Raman spectrum obtained when the incident laser power is 1%, and b) is the Raman spectrum obtained when the incident laser power is 10%. For these three samples, the intensity peak appears when the Raman shift is 520.9cm-1. From this, it can be inferred that the corresponding three sets of infrared pulse laser tests all make the doped silicon wafers in the experiment change from amorphous silicon to crystalline silicon.

4.5 Annealing with green laser

Next, the annealing of a green pulsed laser with a wavelength of 1064nm on the wafer sample will be discussed. The research method is the same as that of infrared laser annealing.

First of all, it needs to be pointed out that this green laser's theoretical beam spot diameter is 0.128 mm by calculation in Chapter 2. Considering that the laser's output is a Gaussian beam, the analysis of BeamGage® can tell that the central area of the Gaussian with a diameter of 0.05mm contains about 11.7% of the total power. It means that the actual laser beam spot area is 1.96×10^{-5} cm^2. The green laser's maximum output power and spot size are smaller than those of the infrared laser.

From multiple tests, three sets of good results were found for further analysis. In order to distinguish the samples annealed by the infrared laser, the names of the samples annealed by the green laser are 1G, 2G, and 3G.

N.	Power [W]	Setted Power [W]	Percentage [%]	Pulse frequency [kHz]	Scan Speed [mm/s]	Interline Hatching [μm]	Pulse width [ns]	Area [cm^2]	Pulse energy [mJ]	Fluence (per pulse) J/cm^2	Peak power [kW]	Irradiance [MW/cm^2]	Laser Dwell [μs]	Overlap scan direction [μm]
1G	0.524	4.48	64.0	20	20	50	10	1.9635E-05	0.026	1.33	2.62	133.48	0.500	1
2G	0.573	4.90	70.0	20	20	50	10	1.9635E-05	0.029	1.46	2.87	145.99	0.500	1
3G	0.622	5.32	76.0	20	20	50	10	1.9635E-05	0.031	1.59	3.11	158.50	0.500	1

Table 4.5.1 Green laser samples

Compared with the infrared laser annealing test, there are no new physical parameters. The output power of the green laser is in the form of a percentage in the software. Considering that the beam spot diameter of the pulsed green laser projected on the silicon wafer surface is 50 μm, Interline Hatching should also be set to 50 μm.

It is easy to know that the green laser does not burn their surfaces by observing these three samples under a microscope. Moreover, uniform tracks are left on the surfaces after the laser scanning, which completely covers the annealed area. See figure 4.5.1.

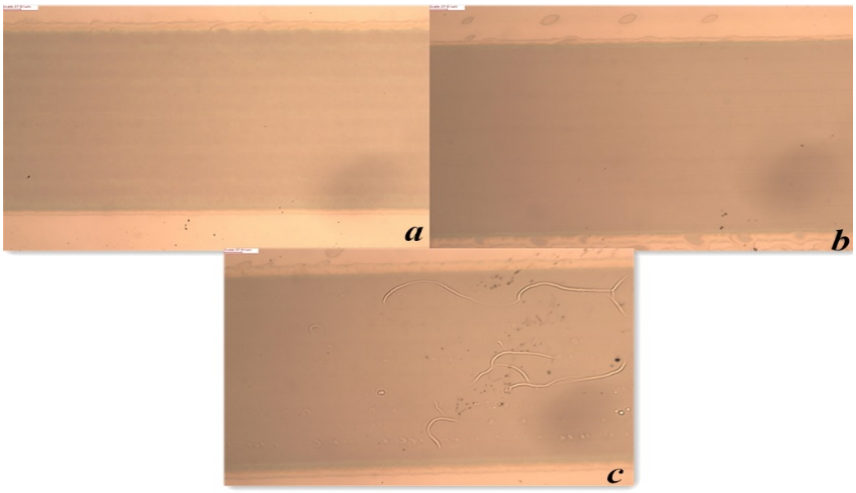

Figure 4.5.1 Green laser samples under microscopic observation. Observe three samples under the microscope, a) represents 1G, b) represents 2G, and c) represents 3G. The surfaces of the three samples were not burnt and had good uniformity.

Further, the profiler is used to detect the modification of the surface by the pulsed green laser. The sampling method and configuration of the profiler are the same as before. No more description here.

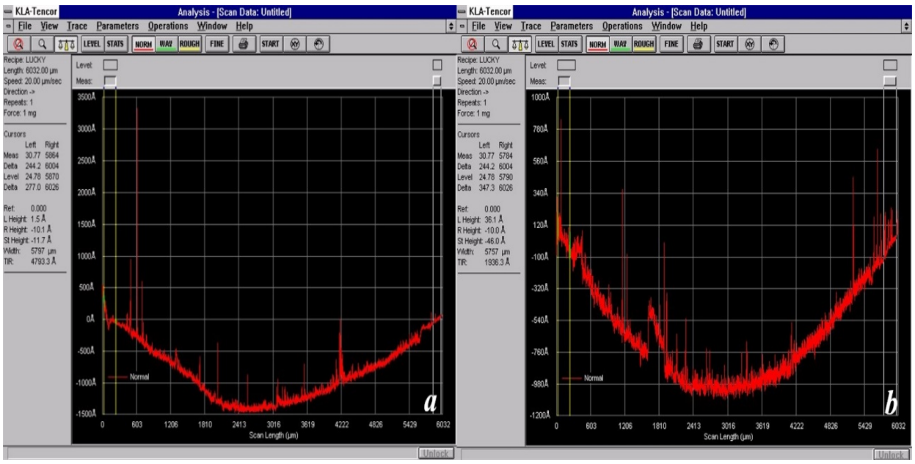

Figure 4.5.2 Profiler results for sample 1G

The sampling length for sample 1G is 6032 µm. In figure 4.5.2, a) represents the probe scanning over the upper part of the silicon wafer, and b) in the right figure is the result of the probe scanning over the lower part of the silicon wafer. It can be seen from the figure that in the centre part of the annealing area, the surface roughness of sample 1G exhibits large vibrations.

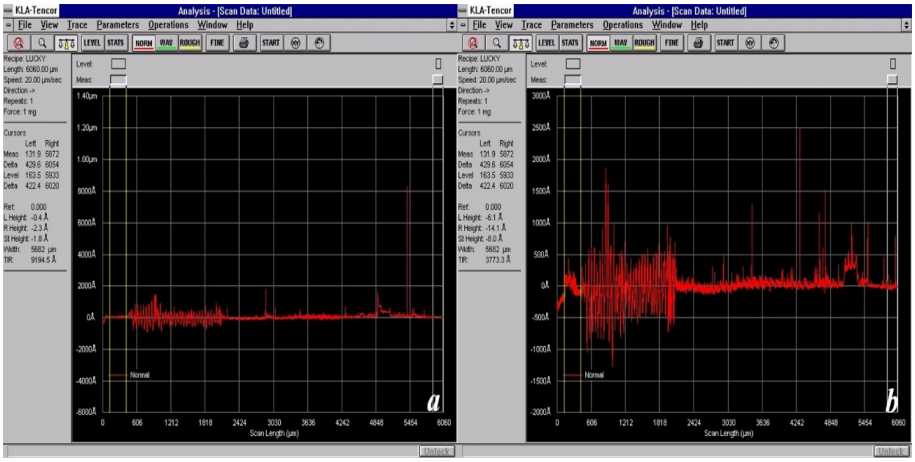

Figure 4.5.3 Profiler results for sample 2G

The sampling length for sample 2G is 6060 µm. In figure 4.5.3, the same mean for a) and b) as 1G. It can be seen from figure 4.5.3 that in the left part of the annealing area, the surface roughness of sample 2G exhibits large vibrations.

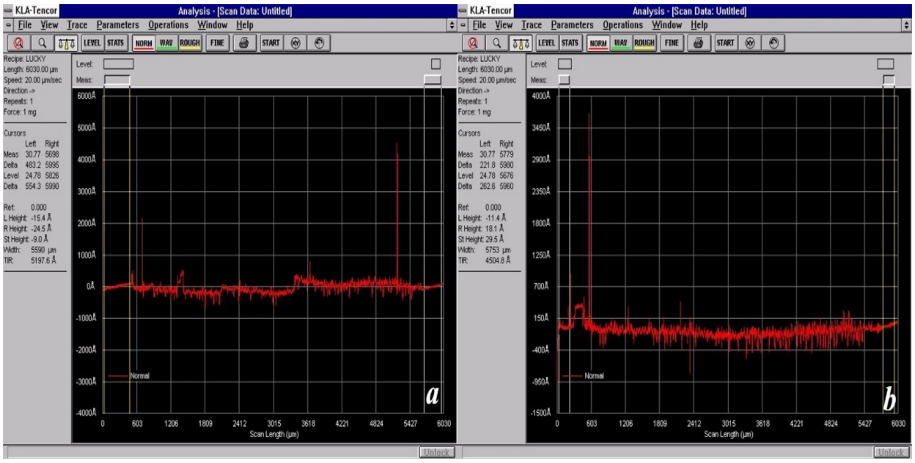

Figure 4.5.4 Profiler results for sample 3G

The sampling length for sample 3G is 6030 µm. In figure 4.5.4, the same meaning for a) and b) as 1G.

Next, use the data generated by the profiler to perform mathematical analysis on these three samples, then make table 4.5.2.

Sample	Location	Sampling Length(μm)	Sampling Points	R_{Max}(Å)	R_A(Å)
1G	1G Upper	6032	15080	4793.26	827.41
1G	1G Lower	6032	15080	1936.30	625.56
2G	2G Upper	6060	15150	9194.49	143.54
2G	2G Lower	6060	15150	3773.34	137.11
3G	3G Upper	6030	15075	5197.60	137.17
3G	3G Lower	6030	15075	4673.71	118.38

Table 4.5.2 Profiler results for Green laser samples

By comparing the data obtained from these three samples and six groups of tests, it can be found that the first sample 2G and the third sample have very small roughness. Their results are better than the first sample 1G, and their results are satisfactory.

Similarly, the Raman spectrum is used to discuss the crystallisation of these three samples. First, perform Raman scattering on the unannealed area of sample 2G and draw the Raman spectrum, as shown in Figure 4.5.5.

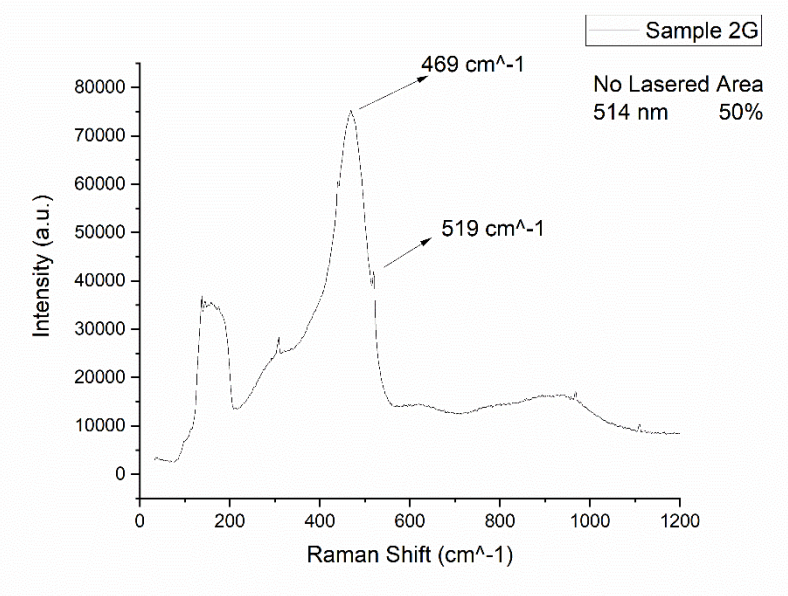

Figure 4.5.5 Raman spectra for the non-annealed region of sample 2G

Similar to the results in the infrared pulsed laser test, the area not irradiated by the laser showed the characteristics of amorphous silicon in the Raman spectrum, as shown in figure 4.5.6. For samples 1G, 2G, and 3G, the Raman spectrum of the area processed by the green pulse laser shows that all samples are converted from amorphous silicon to crystalline silicon.

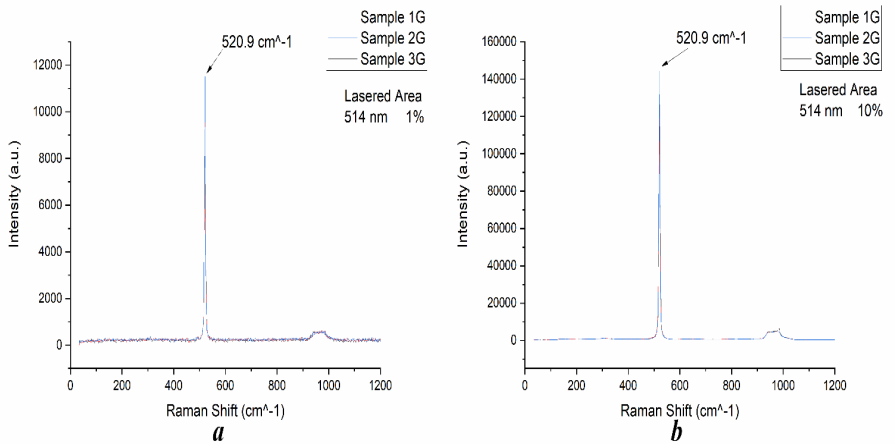

Figure 4.5.6 Raman spectrum for annealed region of Green samples

When the implanted impurity ions damage crystalline silicon, the Raman spectrum will show the distribution of amorphous silicon. Once the silicon wafer temperature reaches 900 °C, the ordered lattice structure will be rebuilt, and the silicon wafer will change from an amorphous state to a crystalline state. All the Raman spectrum above indicates that all doped samples have been crystallised with the action of pulsed infrared laser and pulsed green laser. It can be inferred that all samples have reached at least 900 °C under laser irradiation. For wafer annealing, it needs to be annealed at around 1400 °C, so it is still unknown whether a pulsed laser perfectly anneals these samples. The final result needs to be confirmed by SRP(Spreading resistance profiling) and SIMS(Secondary Ion Mass Spectroscopy).

Chapter 5 Conclusion

This experiment discussed the annealing effect of infrared pulsed laser (1064 nm) and green pulsed laser (532 nm) on phosphorous doped wafers.

A complete 6-inch silicon wafer was cut before annealing. Several small square slices with a side length of 1.27 cm were attempted to be cut from the wafer. The effects of the infrared pulsed laser and the green pulsed laser on the cut edges of the wafers were compared. Considering that the actual spot diameter of the infrared pulsed laser (20 μm) is smaller than that of the green pulsed laser (50 μm), the red pulsed laser produces a smaller range of energy radiation at the cut edge of the silicon wafer. Therefore, it is concluded that the infrared pulsed laser causes fewer defects at the wafer edge than the green pulsed laser and may be more suitable for wafer cutting. Then the cutting of wafers from the front and back using infrared pulsed lasers was tried. The laser parameters were optimised, and the slightest mean defect in the test was 29.10 μm at a fluence of 10.50 J/cm^2 for front side cutting. When cutting from the backside of the wafer, the total number of scans could be reduced, and the scanning speed increased because of the increased laser output.

After cutting the wafers from the backside, the cut square slices are placed in an ultrasonic cleaner, and the positive photoresist is washed off the surface using an acetone solution. Optical lens paper is then used to remove the slag from the front side of the wafer. The effect of the infrared pulsed laser parameters on the wafer edges during the laser cutting process was compared before annealing.

From several wafer samples annealed by infrared pulse laser and green pulse laser, six samples processed under different laser parameters (three from infrared pulse laser and three from green pulse laser) were selected. In the infrared pulsed laser annealing tests, the fluence received by the three samples was 0.66 J/cm^2, 1.07 J/cm^2 and 1.28 J/cm^2, respectively. When using the green pulsed laser, the fluence received by the three samples was 1.33 J/cm^2, 1.46 J/cm^2 and 1.59 J/cm^2, respectively.

Through the optical microscope, it can be known that none of the six samples was burned by the laser, and the scanning traces of the laser evenly covered the designated area. The contact profiler obtained the surface roughness of the annealed areas of six samples.

Analyze the samples before annealing and those after annealing with Raman spectra. It can be known from the Raman spectrum that when the Raman shift is 469 cm^{-1}, the unannealed samples have the maximum intensity peak. For all the annealed samples, the maximum peak intensity peak appears at the Raman shift of 520.9 cm^{-1}. When the Raman shift is 469 cm^{-1}, the samples at this time are still amorphous silicon. When the Raman shift is 520.9 cm^{-1}, it proves that the samples have become crystalline silicon at this moment. All in all, the analysis of the Raman spectra shows that the six samples have been crystalized, and the internal lattice structure of the silicon wafers has been re-formed.

Further confirmation is required from SRP and SIMS as to whether the two pulsed lasers successfully induced the samples to complete annealing.

Bibliography

[1] Mollick, Ethan. (2006). Establishing Moore's Law. Annals of the History of Computing, IEEE. 28. 62 - 75. 10.1109/MAHC.2006.45.

[2] Demenev E. Evolution of Arsenic nanometric distributions in silicon under advanced ion implantation and annealing processes[D]. University of Trento, 2013.

[3] Brown R A, Kononchuk O, Rozgonyi G A, et al. Impurity gettering to secondary defects created by MeV ion implantation in silicon[J]. Journal of applied physics, 1998, 84(5): 2459-2465.

[4] Portavoce A, Simola R, Mangelinck D, et al. Dopant diffusion during amorphous silicon crystallisation [C]//Defect and Diffusion Forum. Trans Tech Publications Ltd, 2007, 264: 33-38.

[5] Zhang Tonghe, Li Guohui, Wu Yuguang. Transient enhanced diffusion model in rapid annealing lattice recovery[J]. Nuclear Techniques, 1988, 10.

[6] Marqués L A, Pelaz L, Aboy M, et al. The laser annealing induced phase transition in silicon: a molecular dynamics study[J]. Nuclear Instruments and Methods in Physics Research Section B: Beam Interactions with Materials and Atoms, 2004, 216: 57-61.

[7] García O, García-Ballesteros J J, Munoz-Martin D, et al. analysis of wavelength influence on a-Si crystallisation processes with nanosecond laser sources[J]. Applied surface science, 2013, 278: 214-218.

[8] Ghosh A K, Fishman C, Feng T. Theory of the electrical and photovoltaic properties of polycrystalline silicon[J]. Journal of Applied Physics, 1980, 51(1): 446-454.

[9] Shen Z, Xin W, Song Y. Progress of research on high energy laser component[C]//Fourth International Symposium on High Power Laser Science and Engineering (HPLSE 2021). International Society for Optics and Photonics, 2021, 11849: 118490W.

[10] Maiman T H. Stimulated optical radiation in ruby[J]. 1960.

[11] Sorokin P P, Stevenson M J. Stimulated infrared emission from trivalent uranium[J]. Physical Review Letters, 1960, 5(12): 557.

[12] Zinth W, Laubereau A, Kaiser W. The long journey to the laser and its rapid development after 1960[J]. The European Physical Journal H, 2011, 36(2): 153-181.

[13] Javan A, Bennett Jr W R, Herriott D R. Population inversion and continuous optical maser oscillation in a gas discharge containing a He-Ne mixture[J]. Physical Review Letters, 1961, 6(3): 106.

[14] Svelto O, Hanna D C. Principles of lasers[M]. New York: Plenum press, 1998.

[15] Lasers.http://labman.phys.utk.edu/phys222core/modules/m11/lasers.html

[16] THE VISIBLE LIGHT SPECTRUM. https://www.once.lighting/visible-light-spectrum/

[17] Specification of IR laser, redENERGY®

[18] https://en.wikipedia.org/wiki/Beam_divergence

[19] User manual of VLASE™ GREEN

[20] "History of the Chip Equipment, Session 5.3: Dicing," VLSI Research, Inc., 1987, retrieved November 23, 2011

[21] Leone, Claudio & Lopresto, V. & Pagano, Nunziante & Genna, Silvio & Iorio, I. (2010). Laser cutting of silicon wafer by pulsed Nd:YAG source.

[22]Ganesh V P, Lee C. Overview and emerging challenges in mechanical dicing of silicon wafers[C]//2006 8th Electronics Packaging Technology Conference. IEEE, 2006: 15-21.
[23]Udi Efrat, "Optimising the Wafer Dicing Process," Proc. International Electronics Manufacturing Technology Syposium, 1993, pp. 245-253.
[24]Koh, Wen Shi & Yow, K.. (2013). The characteristics and factors of a wafer dicing blade and its optimised interactions required for singulating high metal stack lowk wafers. 208-212. 10.1109/EPTC.2013.6745714.
[25]Savriama G. Review of laser technologies for dicing microelectronics chips[J]. Research Gate, 2016.
[26]"Thin wafer processing and dicing equipment market 2016," Yole Development, Tech. Rep., 2016.
[27]Hong, M. and Q. Xie. "Laser Singulation of Thin Wafers & Difficult Processed Substrates: A Niche Area over Saw Dicing." Journal of Laser Micro Nanoengineering 1 (2006): 84-88.
[28]Dunsky C M. Laser material processing in microelectronics manufacturing: status and near-term opportunities[C]//Photon Processing in Microelectronics and Photonics IV. International Society for Optics and Photonics, 2005, 5713: 200-214.
[29]Yang W, Ling L, Lijun Y, et al. Simulation and experimental research on water-jet guided laser cutting silicon wafer[C]//2008 International Conference on Electronic Packaging Technology & High Density Packaging. IEEE, 2008: 1-6.
[30]Lei W S, Kumar A, Yalamanchili R. Die singulation technologies for advanced packaging: A critical review[J]. Journal of Vacuum Science & Technology B, Nanotechnology and Microelectronics: Materials, Processing, Measurement, and Phenomena, 2012, 30(4): 040801.
[31]Evertsen R, Hendriks R. Backside processing steps elimination and cost reduction by multi beam full cut laser dicing[C]//Compound Semiconductor Manufacturing Technology Conference, Palm Springs, CA. 2011: 16-19.
[32]Borkulo J V, Hendriks R. First Multi Beam Full Cut Laser Dicing of Thin Low K Wafers[J]. ECS Transactions, 2010, 27(1): 891.
[33]Lei W S, Kumar A, Yalamanchili R. Die singulation technologies for advanced packaging: A critical review[J]. Journal of Vacuum Science & Technology B, Nanotechnology and Microelectronics: Materials, Processing, Measurement, and Phenomena, 2012, 30(4): 040801.
[34]http://www.hamamatsu.com.cn/UserFiles/upload/file/20181015/SD_tech_TLAS9004E.pdf
[35]Kumagai M, Uchiyama N, Ohmura E, et al. Advanced dicing technology for semiconductor wafer—stealth dicing[J]. IEEE Transactions on Semiconductor Manufacturing, 2007, 20(3): 259-265.
[36]Godbole, V.P., Chaudhari, S.M. Laser annealing of silicon. Bull. Mater. Sci. 11, 97–108 (1988). https://doi.org/10.1007/BF02744548
[37]Alba P A, Aubin J, Perrot S, et al. Solid phase recrystallisation induced by multi-pulse nanosecond laser annealing[J]. Applied Surface Science Advances, 2021, 3: 100053.
[38]Boyd, I., Wilson, J. Laser annealing for semiconductor devices. Nature 287, 278 (1980). https://doi.org/10.1038/287278a0
[39]White C W, Narayan J, Young R T. Laser annealing of ion-implanted semiconductors[J]. Science, 1979, 204(4392): 461-468..

[40]Ukawa K, Kanda Y, Sameshima T, et al. Activation of silicon implanted with phosphorus and boron atoms by infrared semiconductor laser rapid annealing[J]. Japanese Journal of Applied Physics, 2010, 49(7R): 076503.
[41]Schnell, G.; Duenow, U.; Seitz, H. Effect of Laser Pulse Overlap and Scanning Line Overlap on Femtosecond Laser-Structured Ti6Al4V Surfaces. Materials 2020, 13, 969. https://doi.org/10.3390/ma13040969
[42]https://ceas.uc.edu/content/dam/ceas/cleanroom/Manuals/P15%20v7.0%20User%20Manual.pdf.page,63
[43]Gadelmawla, ES & Koura, Monir & Maksoud, Talal & Elewa, Ibrahim & Soliman, Hassan. (2002). Roughness parameters. Journal of Materials Processing Technology. 123. 133-145. 10.1016/S0924-0136(02)00060-2.
[44]Harris D.C. and Bertolucci M.D. (1978) Symmetry and Spectroscopy, an Introduction to Vibrational and Electronic Spectroscopy. Oxford University Press, New York.
[45]Xu Z, He Z, Song Y, et al. Topic review: application of Raman spectroscopy characterisation in micro/nano-machining[J]. Micromachines, 2018, 9(7): 361.